(FE-SEM, S-4700, Hitachi Co., Tokyo, Japan) and surface roughness tester (SV-3000S4, Mitutoyo Co., Japan).

2.5. Animal study

Hardened cylindrical specimens (15 mm in length and 4 mm in diameter) of the cements were subjected to implantation for mechanical test. The specimens were implanted into the femur of nine 2-year-old female beagle dogs weighing 8–11 kg. The guidelines for animal experimentation of Chiba University were carefully observed. They were sedated with an intramuscular injection of Ketamine chloride (10 mg/kg). The cylindrical specimen was inserted into each femur of the dog from the lateral aspect of the diaphysis hemicortically. Specimens were randomly distributed in the femur sites to avoid a positional bias. For histological study, we used six 2-year-old female beagle dogs weighing 8–11 kg. Through the parapatellar approach to the distal femur, the medullary cavity was drilled from this region and intramedullary injection of the cement solutions into the dog femur was performed manually using 20 ml syringe. Icepacin sulfate (200 mg) was administered intramuscularly just before the operation. After the operation, the animals were housed in cages, provided with water and chow, and allowed to move unrestricted at all times. After 3, 5 and 8 weeks, the dogs were sacrificed with an overdose of sodium pentobarbital. The femur with the inserted specimen was removed. The strength of the implant–bone interface was evaluated for six specimens at each determination point using the push-out test. The prepared fresh samples were fixed in a testing jig with resin, and the implants were pushed out from the surrounding bone using a material testing machine (SHIMADZU EHF-F01, Shimadzu Co., Kyoto, Japan) [13]. A loading rate of 0.5 mm/min was used for all tests. A load–displacement curve was recorded to measure the maximum force at breakage, which was defined as the bonding strength between bone and the implant. For the histological study, the dog femur with hardened injected cement was transversely sectioned at the diaphysis. Two samples were examined at each determination point. The interface between cement and bone was also observed by micro-focus X-ray computed tomography (micro-CT; MCT-CB130MF, Hitachi medical Co., Japan). The samples were soaked in 70 mass% ethanol solution for fixation. They were dehydrated by consecutive soaking for 1 day in each solution of a graded ethanol/water system (ethanol/water: 70/30, 80/20, 90/10, 95/5, 97/3, and 100/0 in mass ratio). The dried specimens were embedded in epoxy resin. A 200-μm cross-section was cut from the specimen and mounted on a slide glass, followed by polishing to a thickness of approximately 30 μm. Toluidine blue staining and Villannueva–Goldner staining were performed to observe the surrounding bone reaction under an optical microscope. For the histological study, calcified bone in the interstices between cortex bone and cement surface were measured by analyzing software Winroof® (Mitani Co., Japan) at 8 weeks. Regions of interest (ROIs) were defined as exactly the same size (1.1 mm × 1.1 mm) in all samples and two regions of each sample were measured.

2.6. Statistical analysis

Values were expressed as the mean±standard deviation (SD). Statistical differences were analyzed with the use of the Mann Whitney U test; $p<0.05$ was considered statistically significant. Two of the specimens for push-out test were infected and four specimens were implanted incorrectly. So we discarded these specimens, and the final numbers (n) were 6, 3 and 4 for modified PMMA and 6, 4 and 5 for conventional one at 3, 5 and 8 weeks after implantation, respectively.

3. Results

Table 2 gives the maximum temperature during setting of the bone cements and their setting time. The setting time of the modified cement was longer than that of conventional PMMA bone cement (Zimmer® bone cement), while the maximum temperature during the setting of the modified cement was lower. Fig. 1 shows the compressive strength of the cements with or without soaking in SBF for 7 days. The compressive strength of the modified cement without soaking in SBF was almost the same as the conventional one, but when soaked in SBF, it decreased and did not satisfy the value required by ISO5833 (70 MPa). Fig. 2 shows SEM photographs of the surface of the cements before and after soaking in SBF for various periods. Aggregations of tiny particles were newly observed on the surface of the modified cement soaked in SBF for 1 day, whereas no significant changes were observed on the surface of the Zimmer® bone cement. Fig. 3 shows TF-XRD patterns of the cements with and without soaking in SBF for various periods up to 7 days. Peaks assigned to hydroxyapatite (JCPDS#15-0876) with low crystallinity were detected approximately at $2\theta = 32°$ for modified cement, while Zimmer® bone cement showed peaks assigned to barium sulfate (JCPDS#24-1035). These results indicate that the apatite crystals with fine particles were deposited on the surface of the modified cement within 1 day after soaking in SBF, to form a layer of hydroxyapatite on the modified cement. In contrast, Zimmer® bone cement did not show any apatite formation after exposure to SBF. Table 3 shows surface roughness of the cements with and without soaking in SBF for 1, 3 and 7 days. Surface roughness (Ra) of the modified PMMA bone

Table 2
Maximum temperature during polymerization and setting time

Sample	Maximum temperature (°C, mean±SD)	Setting time (min, means±SD)
Zimmer® bone cement	82.5±0.6	12.0±0.4
Modified PMMA bone cement	51.0±1.2	18.1±2.3

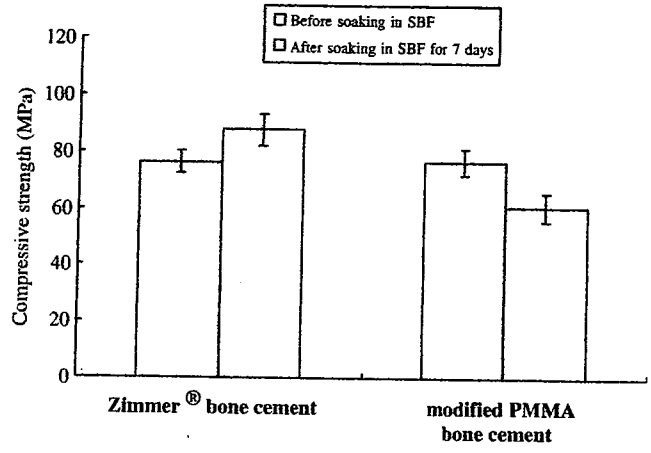

Fig. 1. The compressive strength of the cements with or without exposure to simulated body fluid (SBF).

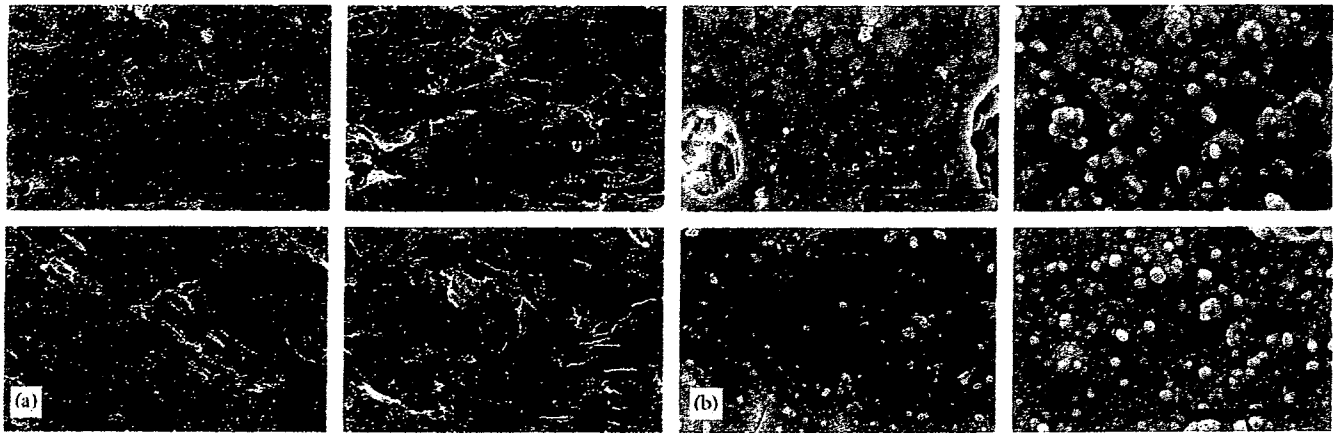

Fig. 2. SEM photographs of the surfaces of (a) Zimmer® bone cement and (b) the modified PMMA bone cement, after soaking in simulated body fluid (SBF) for 1, 3 and 7 days. "0d" indicates the specimen without soaking in SBF.

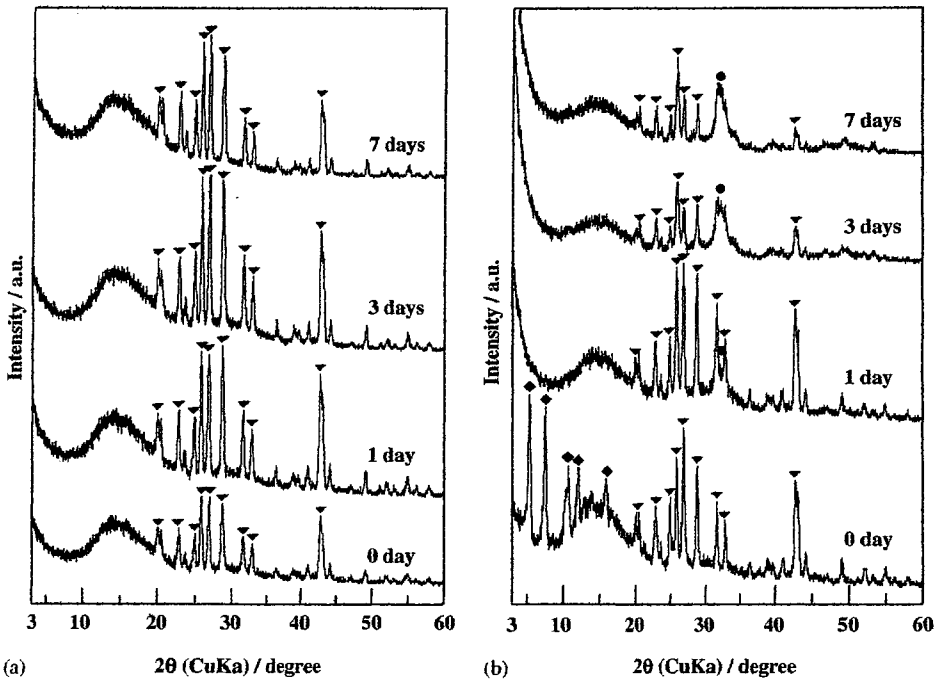

Fig. 3. TF-XRD patterns of the cements with and without soaking in simulated body fluid (SBF) for 1, 3 and 7 days. "0 day" indicates the specimen without soaking in SBF. Black circle: hydroxyapatite (JCPDS#15-0876); black triangle: barium sulfate (JCPDS#24-1035); black diamond: calcium acetate · $0.5H_2O$ (JCPDS#19-0199): (a) Zimmer® bone cement and (b) modified PMMA bone cement.

Table 3
Surface roughness of cements (Ra; mm) with and without soaking in simulated body fluid (SBF) for 1, 3 and 7 days

Sample	Surface roughness of cements (Ra;mm)			
	0 day	1 day	3 days	7 days
Zimmer® bone cement	0.729±0.09	0.882±0.23	0.576±0.08	0.681±0.05
Modified PMMA bone cement	0.316±0.05	1.023±0.10	1.297±0.24	3.385±0.30

cement distinctly increased with increasing soaking periods in SBF, whereas Zimmer® bone cement did not.

Fig. 4 shows the results of push-out test after 3, 5 and 8 weeks implantation of the modified PMMA bone cement, in comparison with those of Zimmer® bone cement. Although the condition differed from the actual clinical application in which the cement is inserted before setting, a significantly higher binding strength ($p<0.05$) was

observed for the modified PMMA bone cement than Zimmer® bone cement, at each implantation period. The push-out load of the modified PMMA bone cement reached 1.60 MPa in 3 weeks, which was maintained up to 8 weeks after implantation, while those of Zimmer® bone cement remained low throughout the examined periods in this study. This result clarifies that the modified PMMA bone cement results in tight fixation with greater strength than conventional PMMA bone cement. In the area where there was a gap between the bone cortex and the surface of modified PMMA, micro-CT and microscopic images showed new bone formation and lamellar bone bridges in all animals 8 weeks after implantation (Fig. 5). On the other hand, little new bone formation was observed for the Zimmer® bone cement. Fig. 6 shows the percentage fraction of the calcified bone in the interstices between cortex bone and cement surface measured by the analyzing software Winroof® in 8 weeks' samples. The percentage fraction of the calcified bone around the modified PMMA bone cement was significantly larger than Zimmer® bone cement ($p = 0.02$). These evidences support the finding that the higher strength on the push-out test for modified PMMA is attributed to higher affinity, which is osteoconduction, of the modified PMMA bone cement to bone than that of the conventional PMMA bone cement.

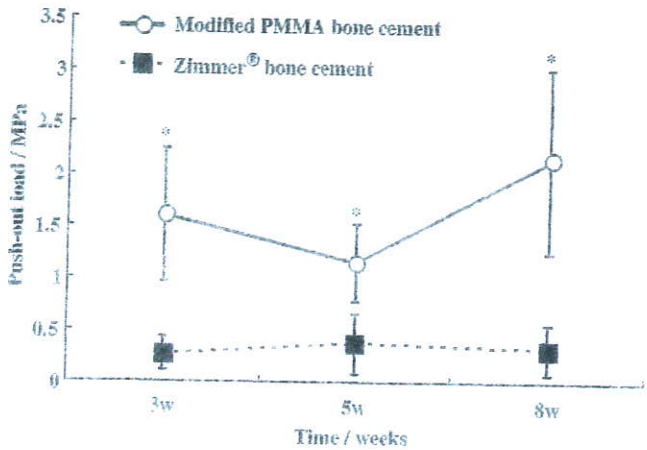

Fig. 4. Results of push-out strength after implantation in dog femur. A significantly higher binding strength ($p<0.05$) was observed for the modified PMMA bone cement compared to Zimmer® bone cement (conventional PMMA bone cement), at each implantation period.

4. Discussion

To develop a bioactive PMMA-based bone cement, an optimal composition was sought to obtain adequate mechanical strength and handling properties. Additives for inducing bioactivity on bone cement should not affect the workability of the bone cement. Previous reports on modifications of PMMA bone cement with MPS and

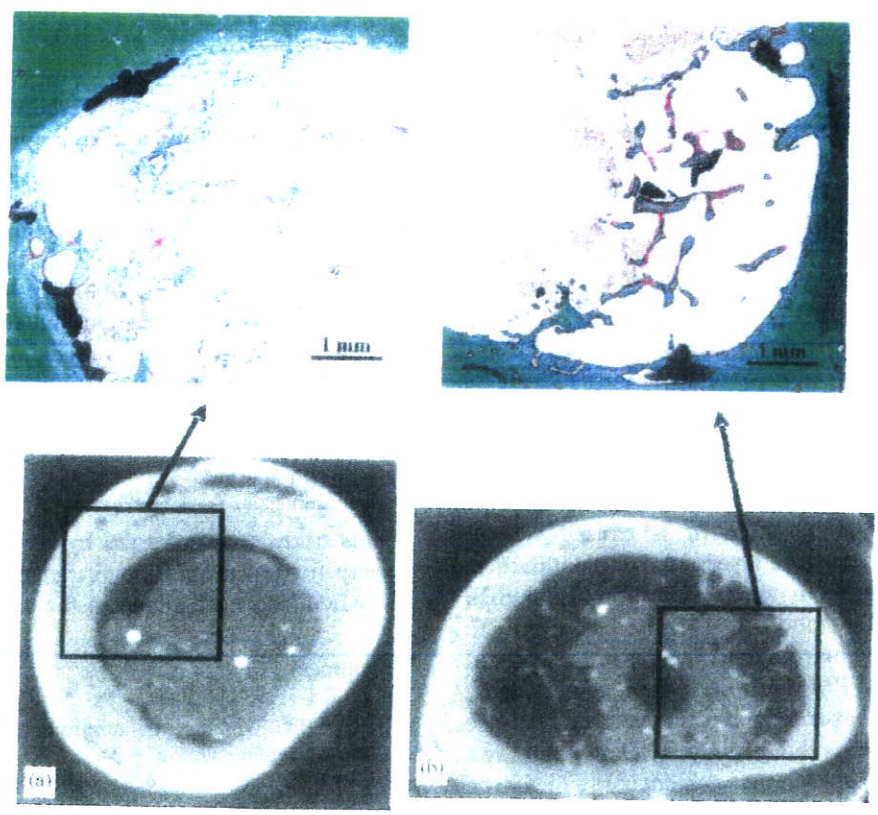

Fig. 5. Images of micro-focus X-ray computed tomograms (micro-CT) at 8 weeks after implantation, in comparison with microscopic images (Villanueva–Goldner stain ×1): (a) Zimmer® bone cement and (b) modified PMMA bone cement.

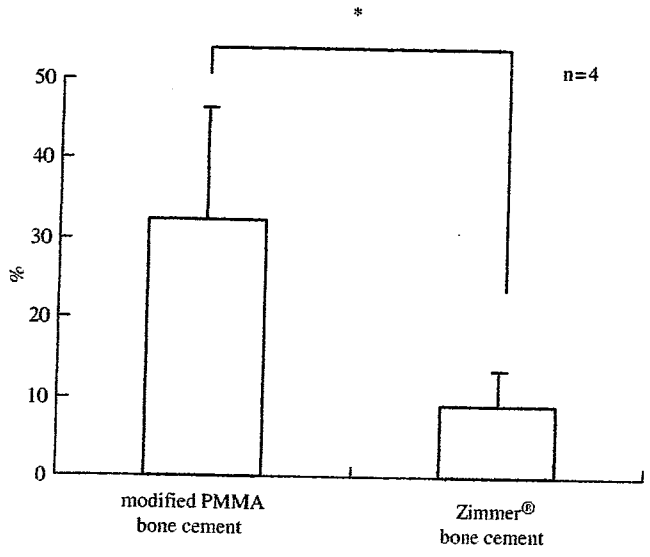

Fig. 6. Results of the percentage fraction of the calcified bone in the interstices between cortex bone and cement surface at 8 weeks. More calcified bone ($^*p<0.05$) was observed for the modified PMMA bone cement compared to Zimmer® bone cement (conventional PMMA bone cement). Measured by analyzing software Winroof® ($n = 4$).

calcium salts showed prolonged setting time and reduced mechanical strength after the modification [8,14]. These problems can be solved by selecting the appropriate calcium salts [10]. In this study, it was confirmed that MPS and heat-treated calcium acetate could be the appropriate candidates for modification, because the setting time was within 20 min and there was minimal heat generation during polymerization as shown in Table 2. Incorporation of MPS reduced the polymerization rate, compared to MMA liquid alone. The reduction in the compressive strength from approximately 75 to 65 MPa due to exposure to SBF, which does not meet the mechanical properties required by ISO 5833, remains a problem to be solved.

The findings of the present study suggested that the modification of PMMA bone cement with 20 mass% of MPS and calcium acetate resulted in high biological affinity to living bone. Thus, a higher binding strength could be achieved between the modified PMMA bone cement and living bone than for the conventional PMMA bone cement. The binding strength is caused by the formation of a hydroxyapatite layer after implantation in the bony defect, because in vitro evaluation using SBF clearly showed that the modified cement had ability to form apatite in body environment. Therefore, osteoconduction of the modified PMMA bone cement is induced by the formation of the apatite layer through the surface reaction with surrounding body fluids after implantation of the modified PMMA bone cement. In fact, the animal study indicated that there was extensive new bone formation around the modified PMMA bone cement, and that direct bone apposition to the modified PMMA bone cement surface was observed on histological examination. Micro-CT images also showed bridges of new bone from the bone cortex to the surface of the modified PMMA bone cement that had developed into lamellar bone 8 weeks after implantation. This in vivo evidence confirms the fact that modified PMMA bone cement has higher affinity to living bone tissue, than the conventional PMMA bone cement. In contrast, conventional PMMA bone cement is more stable in chemical reaction to body fluids than the modified one. The stability of the conventional PMMA bone cement in body environment is confirmed from the results of TF-XRD, SEM and surface roughness, as seen in Figs. 2 and 3 as well as Table 3. Although the modifications with MPS and calcium acetate make the PMMA bone cement bioactive, dissolution of the components, probably calcium acetate and part of hydrolyzed MPS, results in a decrease in compressive strength of the cement as shown in Fig. 1. The increase in the surface roughness of the modified PMMA bone cement shown in Table 3 is attributed to dissolution of the calcium acetate from the bone cement and/or deposition of apatite crystals, through reaction of the cement with SBF. Increased surface roughness may contribute to an increase in binding strength between the cement and living bone due to anchoring effects. On the other hand, the toxicity of the dissolved components should be clarified in future studies. Long-term stability after implantation should be clarified in order to achieve successful application.

5. Conclusion

The results of this study show that higher bonding strength between bone and implant can be achieved with modified PMMA bone cements. Histological observation and micro-CT images showed that the PMMA cement modified with γ-methacryloxypropyl trimethoxysilane (MPS) and calcium acetate exhibits osteoconductive properties, whereas the conventional PMMA bone cement did not. This type of chemical modification was effective in providing PMMA bone cement with bioactivity, thus developing a new bioactive bone cement with a potential for much stable fixation in a short period after implantation.

Acknowledgments

This study was supported by a grant from the Japanese Society for the Promotion of Science. The authors thank Mr. Michihiro for his help in the animal study.

References

[1] Hench LL, Wilson J. An introduction to bioceramics. Singapore: World Scientific; 1993. p. 1–24.
[2] Harper EJ. Bioactive bone cements. Proc Inst Mech Eng H 1998;212:113–20.
[3] Shinzato S, Kobayashi M, Mousa WF, Kamimura M, Neo M, Kitamura Y, et al. Bioactive polymethylmethacrylate-based bone cement: comparison of glass beads, apatite- and wollastonite-containing

glass–ceramic, and hydroxyapatite fillers on mechanical and biological properties. J Biomed Mater Res 2000;51:258–72.
[4] Shinzato S, Nakamura T, Kokubo T, Kitamura Y. A new bioactive bone cement: effect of glass bead filler content on mechanical and biological properties. J Biomed Mater Res 2001; 54:491–500.
[5] Kokubo T. Recent progress in glass-based materials for biomedical applications. J Ceram Soc Japan 1991;99:965–73.
[6] Kim HM. Bioactive ceramics: challenges and perspectives. J Ceram Soc Japan 2001;109:S49–57.
[7] Ohtsuki C, Kokubo T, Yamamuro T. Mechanism of apatite formation on $CaO–SiO_2–P_2O_5$ glasses in a simulated body fluid. J Non-Cryst Solids 1992;143:84–92.
[8] Ohtsuki C, Miyazaki T, Kyomoto M, Tanihara M, Osaka A. Development of bioactive PMMA-based cement by modification with alkoxysilane and calcium salt. J Mater Sci Mater Med 2001; 12:895–9.
[9] Mori A, Ohtsuki C, Miyazaki T, Sugino A, Tanihara M, Kuramoto K, et al. Synthesis of bioactive PMMA bone cement via modification with methacryloxypropyltrimethoxysilane and calcium acetate. J Mater Sci Mater Med 2005;16:713–8.
[10] Mori A, Ohtsuki C, Miyazaki T, Sugino A, Tanihara M, Kuramoto K, et al. Synthesis of bioactive PMMA bone cement via modification with methacryloxypropyltrimethoxysilane and calcium acetate. J Mater Sci Mater Med 2005;16:713–8.
[11] ISO. International standard 5833/2: implants for surgery acrylic resin cements. Orthopaedic application, 1992.
[12] Kokubo T, Kushitani H, Sakka S, Kitsugi T, Yamamuro T. Solutions able to reproduce in vivo surface-structure changes in bioactive glass ceramic A-W. J Biomed Mater Res 1990;24:721–34.
[13] Nishimura N, Taguchi T, Yamamuro T, Nakamura T, Kokubo T, Yoshihara S. A study of the bioactive bone cement–bone cement interface: quantitative and histological evaluation. J Appl Biomater 1993;4:29–38.
[14] Miyazaki T, Ohtsuki C, Kyomoto M, Tanihara M, Mori A, Kuramoto K. Bioactive PMMA bone cement prepared by modification with methacryloxypropyltrimethoxysilane and calcium chloride. J Biomed Mater Res 2003;67A:1417–23.

DOI: 10.1002/cmdc.200600008

A PEG-Based Biocompatible Block Catiomer with High Buffering Capacity for the Construction of Polyplex Micelles Showing Efficient Gene Transfer toward Primary Cells

Naoki Kanayama,[a, d] Shigeto Fukushima,[a, c] Nobuhiro Nishiyama,*[b] Keiji Itaka,[b] Woo-Dong Jang,[a] Kanjiro Miyata,[a] Yuichi Yamasaki,[a, d] Ung-il Chung,[b] and Kazunori Kataoka*[a, b, d]

Nonviral gene vectors from synthetic catiomers (polyplexes) are a promising alternative to viral vectors. In particular, many recent efforts have been devoted to the construction of biocompatible polyplexes for in vivo nonviral gene therapy. A promising approach in this regard is the use of poly(ethylene glycol) (PEG)-based block catiomers, which form a nanoscaled core–shell polyplex with biocompatible PEG palisades. In this study, a series of PEG-based block catiomers with different amine functionalities were newly prepared by a simple and affordable synthetic procedure based on an aminolysis reaction, and their utility as gene carriers was investigated. This study revealed that the block catiomers carrying the ethylenediamine unit at the side chain are capable of efficient and less toxic transfection even toward primary cells, highlighting critical structural factors of the cationic units in the construction of polyplex-type gene vectors. Moreover, the availability of the polyplex micelle for transfection with primary osteoblasts will facilitate its use for bone regeneration in vivo mediated by nonviral gene transfection.

Introduction

Gene therapy is a promising approach for the treatment of genetic and intractable diseases and for tissue engineering; however, its success still strongly depends on the development of useful gene vectors.[1] Recently, nonviral vectors based on the complexation of plasmid DNA (pDNA) with synthetic cationic polymers (catiomers) have attracted a great deal of attention as an alternative to viral vectors.[2–4] These vectors, the so-called polyplexes, are aimed toward both efficient transfection and decreased cytotoxicity.[5,6] In particular, there has recently been a strong impetus toward engineering the constituent catiomers to construct biocompatible polyplexes suitable for gene delivery in vivo.[2,5] A promising approach in this regard is the block copolymerization of catiomers with poly(ethylene glycol) (PEG) to obtain PEG-*block*-catiomers, as they spontaneously associate with pDNA to form polyplex micelles at the sub-100-nm scale with a dense and hydrophilic PEG palisade surrounding the polyplex core (Figure 1).[7–10] These polyplex micelles with PEG palisades showed high colloidal stability under physiological conditions and afforded appreciable levels of reporter-gene expression to various cell lines even after preincubation in a serum-containing medium.[7] Notably, the polyplex micelles demonstrated longevity in blood circulation,[11] offering the possibility of their use in systemic gene delivery. Nevertheless, a major obstacle to the successful application of this biocompatible nonviral vector system remains: the limited transfection efficacy toward primary cells.

Herein, we report a novel approach to obtain PEG-*block*-catiomers with remarkably high transfecting activity even toward primary cells, which are known to be sensitive to the toxicity induced by conventional polyplexes. The synthetic strategy for novel block catiomers is based on our unprecedented finding that the flanking benzyl ester groups of poly(β-benzyl L-aspar-

[a] Dr. N. Kanayama, S. Fukushima, Dr. W.-D. Jang, K. Miyata, Dr. Y. Yamasaki, Prof. Dr. K. Kataoka
Department of Materials Engineering
Graduate School of Engineering
The University of Tokyo
Tokyo 113-8656 (Japan)
Fax: (+81)3-5841-7139
E-mail: kataoka@bmw.t.u-tokyo.ac.jp

[b] Dr. N. Nishiyama, Dr. K. Itaka, Prof. Dr. U.-i. Chung, Prof. Dr. K. Kataoka
Center for Disease Biology and Integrative Medicine
Graduate School of Medicine
The University of Tokyo, Tokyo 113-0033 (Japan)
Fax: (+81)3-5841-7139
E-mail: nishiyama@bmw.t.u-tokyo.ac.jp

[c] S. Fukushima
R&D Division, Pharmaceuticals Group
Nippon Kayaku Co., Ltd. (Japan)

[d] Dr. N. Kanayama, Dr. Y. Yamasaki, Prof. Dr. K. Kataoka
Core Research for Evolutional Science and Technology (CREST), Japan Science and Technology Agency (JST) (Japan)

Supporting information for this article is available on the WWW under http://www.chemmedchem.org or from the author.

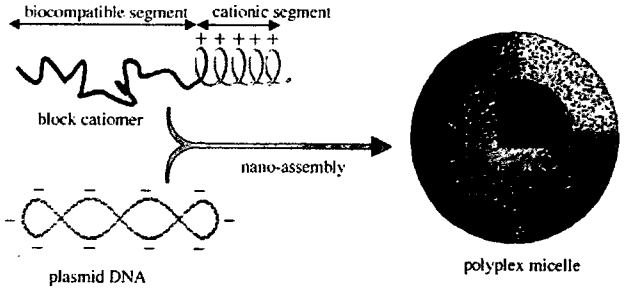

Figure 1. Formation of polyplex micelles through the electrostatic interaction between block catiomers and plasmid DNA.

tate) (PBLA) can undergo a quantitative aminolysis reaction with various polyamine compounds under mild anhydrous conditions at 40 °C, thus allowing the preparation of cationic polyaspartamides with different amine functionalities, yet with the same molecular weight and distribution (Scheme 1). In par-

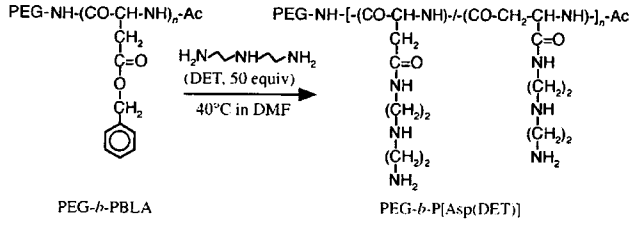

Scheme 1. Synthesis of PEG-*b*-P[Asp(DET)] block catiomer through the aminolysis of PEG-*b*-PBLA. DMF = *N*,*N*-dimethylformamide.

ticular, this study is focused on the unique properties of the ethylenediamine unit integrated into the polyaspartamide side chain. Notably, ethylenediamine is known to undergo a clear two-step protonation with a distinctive *gauche–anti* conformational transition as depicted in Scheme 2,[12] and is thus expected to provide an effective buffering function in the acidic en-

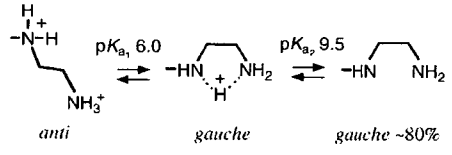

Scheme 2. Two-step protonation of the ethylenediamine unit with a distinctive *gauche–anti* conformational transition.

dosomal compartment (pH 5). It has been suggested that catiomers with a low pK_a value such as polyethylenimine could buffer endosomal acidification and cause an increase in osmotic pressure in the endosome, leading to the disruption of the endosomal membrane to facilitate polyplex transport into the cytoplasm (the so-called proton sponge effect[13]). Indeed, PEG-*block*-polyaspartamide with an ethylenediamine unit at the side chain (PEG-*b*-P[Asp(DET)]) showed a remarkably high transfection efficacy to various cancer cells as well as mouse primary osteoblast cells. Importantly, this block catiomer was found to have remarkably low toxicity, facilitating its use for in vivo gene therapy.

Results and Discussion

PEG-*b*-polyaspartamide carrying the *N*-(2-aminoethyl)aminoethyl group $-(CH_2)_2NH(CH_2)_2NH_2$ as the side chain (PEG-*b*-P[Asp(DET)]) was prepared by the aminolysis of PEG-*b*-PBLA in dry DMF at 40 °C for 24 h in the presence of a molar excess (50 equiv relative to benzyl groups) of diethylenetriamine (DET) (Scheme 1). The ^{1}H NMR spectrum of PEG-*b*-P[Asp(DET)] is shown in Figure 2, and the ^{13}C NMR spectrum is available in

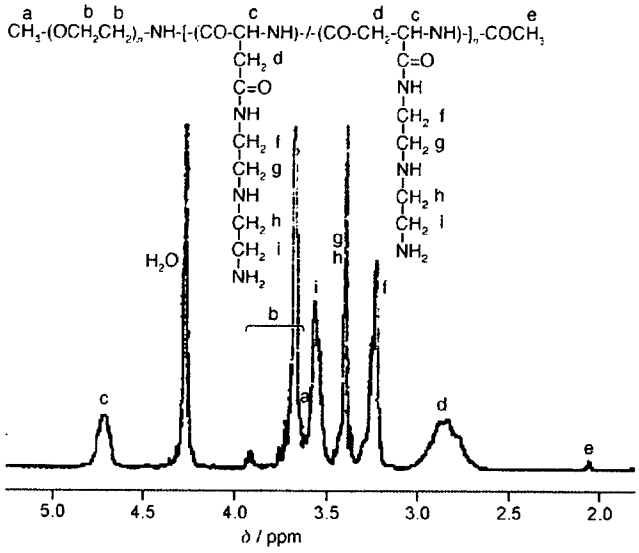

Figure 2. ^{1}H NMR spectrum of PEG-*b*-P[Asp(DET)] (solvent: D_2O, T = 80 °C); the polymer is in a salt form.

the Supporting Information. These data indicate that the aminolysis of the PBLA benzyl groups proceeded in a selective manner to the primary amine moiety of DET. Also, comparison of the integration ratio of the proton peaks (b and f–i) in Figure 2 reveals quantitative introduction of DET into the side chain of PBLA, and a unimodal molecular weight distribution of the obtained polymer was revealed by size-exclusion chromatography (SEC) measurement (Supporting Information). These results suggest a minimal occurrence of inter- or intrapolymer cross-linking by DET during aminolysis. Note that the peaks from the carbonyl and methylene groups of the aspartamide units in the ^{13}C NMR spectrum (Figure S1, Supporting Information) are split into two peaks, suggesting that the aminolysis of PBLA might induce intramolecular isomerization of the aspartamide units to form β-aspartamide. Figure 3 shows the time course of the aminolysis reaction of PBLA with DET, which was evaluated from the change in the ratio of the proton peak integration (f over b) in the ^{1}H NMR spectrum (Figure 2). This result indicates a fast and quantitative aminolysis of PBLA, which is in marked contrast to the lack of aminolysis with poly(γ-benzyl L-glutamate) (PBLG) under the same re-

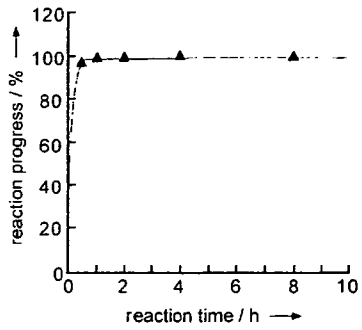

Figure 3. Time course of the aminolysis of PEG-*b*-PBLA with DET in DMF at 40 °C. The reaction progress was estimated from the change in the ratio of the proton peak integration (f over b) in the ^{1}H NMR spectrum (Figure 2).

action conditions (data not shown), highlighting a unique mechanism involved in the aminolysis of PBLA under mild conditions. Presumably, the amide groups of the main chain interact with the carbonyl group of the side chain, which may facilitate the aminolysis reaction.[14] The details of the mechanism of this unique aminolysis reaction are now under investigation in our research group and will be reported elsewhere.

The pH-dependent protonation of PEG-*b*-P[Asp(DET)] in media containing 150 mM NaCl was evaluated by potentiometric titration. The α/pH curve shown in Figure 4 clearly indicates

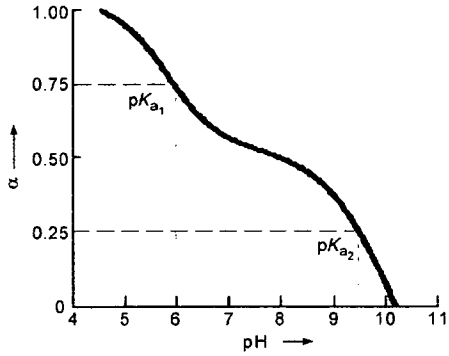

Figure 4. Degree of protonation (α) as a function of pH (α/pH curve) for the PEG-*b*-P[Asp(DET)] block catiomer (150 mM NaCl, aq, 25 °C).

the two-step protonation behavior of PEG-*b*-P[Asp(DET)], which is attributable to the two-step protonation of the ethylenediamine moiety with a distinctive *gauche–anti* conformational transition as indicated in Scheme 2. The two distinct pK_a values of the ethylenediamine moiety in the side chain of polyaspartamide were determined to be 6.0 and 9.5. Notably, this group remains nearly 100% populated by the mono-protonated state (*gauche* form) at pH 7.4, and is capable of exerting a substantial buffering effect in the pH range down to 5.0, at which point the equilibrium shifts to the di-protonated state (*anti* form) (Scheme 2).

The polyplex micelle was prepared by mixing solutions of PEG-*b*-P[Asp(DET)] and pDNA in various ratios of *N/P*, for which *N* is the total number of amine groups in the block catiomer and *P* represents the number of phosphate units in the pDNA. The formation of the polyplex, which accompanies pDNA condensation, was followed by an ethidium bromide (EtBr) dye-exclusion assay at different pH values. As shown in Figure 5, the

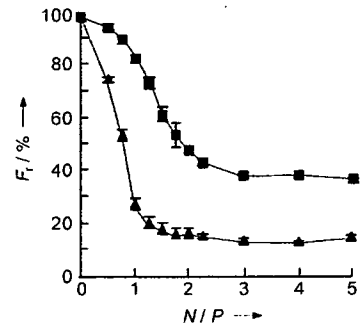

Figure 5. Effect of pH (▲: pH 5.0, ■: pH 7.4) on the relative fluorescence intensity (F_r) of EtBr in solution with pDNA and PEG-*b*-P[Asp(DET)] at various *N/P* ratios.

fluorescence intensity of EtBr decreases with an increase in the *N/P* ratio. At pH 5.0, the fluorescence of EtBr levels off at *N/P* = 1, which is consistent with approximately 95% protonation of the ethylenediamine unit, as expected from the α/pH curve in Figure 4. On the other hand, at pH 7.4, substantial quenching occurred at $N/P \approx 2.0$, which is consistent with the hypothesis that the mono-protonated form of the ethylenediamine unit in PEG-*b*-P[Asp(DET)] might be maintained even inside the polyplex. It is possible that the stabilized *gauche* conformation (Scheme 2) of the mono-protonated form may prevent the ethylenediamine unit from further protonation facilitated by the zipper effect or the local electrostatic field effect in the complexation process with anionic pDNA at pH 7.4.[15] The cumulant diameters and ζ potentials of the polyplexes prepared at different *N/P* ratios are shown in Figure 6. The cumulant diameters of the polyplex micelles were determined to be 70–90 nm throughout the range of the examined *N/P* ratios of 1–20, and the ζ potentials of the polyplexes increased with *N/P* ratios and leveled off at $N/P = 2$ (Figure 6). At $N/P > 2$, the polyplexes were observed to have small absolute ζ potentials (~8 mV), suggesting a core–shell architecture with a hydrophilic and neutral PEG shell surrounding the polyplex core.

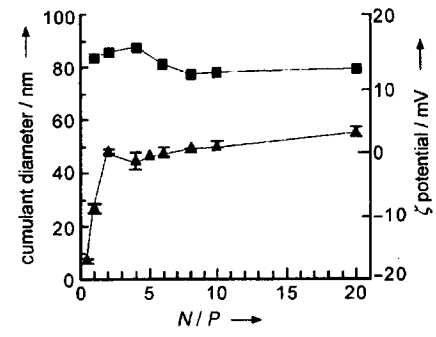

Figure 6. Cumulant diameter (■) and ζ potential (▲) of the PEG-*b*-P[Asp(DET)] polyplex micelles as a function of *N/P* ratio.

The in vitro transfection efficiency (TE) against human hepatoma HuH-7 cells was assessed by a luciferase assay (Figure 7). Notably, a similar trend in TE was also observed for human kidney 293T cells (Supporting Information). In this experiment,

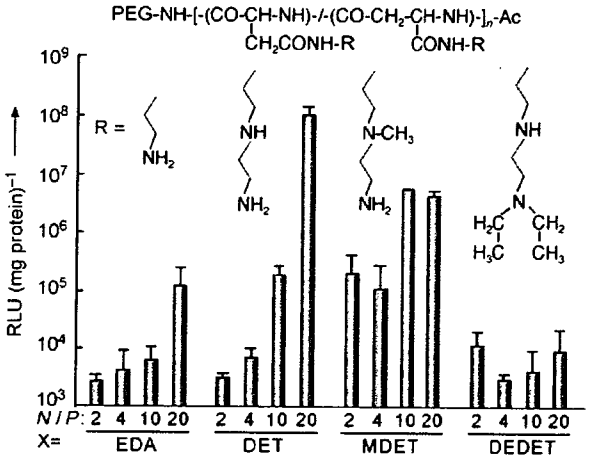

Figure 7. In vitro transfection of the luciferase gene into HuH-7 cells by polyplex micelles from PEG-*b*-polyaspartamides carrying various polyamine components in the side chain (PEG-*b*-P[Asp(X)]) with varying *N/P* ratios. Transfection is reported in relative light units (RLU) per mg protein. The cells were incubated with each polyplex in the medium containing 10% serum for 24 h, followed by incubation for a further 24 h in the absence of polyplex.

the PEG-*b*-P[Asp(DET)]–pDNA micelle was compared with the polyplex micelles from various PEG-*b*-polyaspartamide catiomers made by the similar aminolysis of PEG-PBLA with different amine compounds, with the aim to highlight the unique nature of the P[Asp(DET)] segment. Note that the polyplex micelles from each block catiomer prepared in this study showed sizes and ζ potentials similar to those of the polyplex micelle from PEG-*b*-P[Asp(DET)] (data not shown). The polyplex micelle from the block catiomer with the 2-aminoethyl group $-(CH_2)_2NH_2$ (pK_a 9.4) in the side chain (PEG-*b*-P[Asp(EDA)]), which was prepared through the aminolysis of PEG-*b*-PBLA with ethylenediamine (EDA), showed only 1/10000 of the TE compared with the PEG-*b*-P[Asp(DET)] polyplex micelle at $N/P = 20$. This is presumably due to the impaired buffering capacity of the $-(CH_2)_2NH_2$ unit with the high pK_a value of 9.4 in the experimental pH range as well as to the weak ability of PEG-*b*-P[Asp(EDA)] to condense pDNA based on the EtBr exclusion assay (data not shown).

The TE of the PEG-*b*-P[Asp(DET)] polyplex micelle was further compared with those of the polyplex micelles from the PEG-*b*-polyaspartamide catiomers carrying the N-alkylated ethylenediamine units in the side chain to explore the structural features of the polyplex micelles that are important for effective gene transfection (Figure 7). These block catiomers, PEG-*b*-P[Asp(MDET)] and PEG-*b*-P[Asp(DEDET)], are prepared by the aminolysis reaction of PEG-PBLA with the corresponding amine compounds, 4-methyldiethylenetriamine (MDET) and *N,N*-diethyldiethylenetriamine (DEDET), respectively. Both the PEG-*b*-P[Asp(MDET)] and PEG-*b*-P[Asp(DEDET)] polyplex micelles showed an appreciably lower TE than the PEG-*b*-P[Asp(DET)] polyplex micelle, particularly at higher *N/P* ratios (Figure 7). This result, which highlights the critical sensitivity of TE toward subtle changes in catiomer structure, indicates that additional structural factors, besides distinct pK_a values, play a substantial role in determining the TE of the polyplex micelles constructed from the PEG-*b*-polyaspartamide catiomers carrying the derivatized ethylenediamine units as a side chain; further study is needed to clarify the detailed mechanisms.

The cytotoxicity of the polyplex-forming catiomers is also a crucial aspect for successful nonviral gene therapy. In this regard, all the polyplex micelles from each block catiomer shown in Figure 7 elicited no appreciable cytotoxicity toward HuH-7 cells under the same conditions used for gene transfection (data not shown). Notably, the polyplex micelle from PEG-*b*-P[Asp(DET)] showed remarkably low cytotoxicity despite its efficiency in gene transfection. Therefore, the intrinsic cytotoxicity of PEG-*b*-P[Asp(DET)] catiomer was further assessed against HuH-7 cells, and compared with that of branched polyethylenimine (BPEI, 25 kDa, Aldrich Chemical, USA) and linear polyethylenimine (LPEI, 22 kDa, ExGen500, MBI Fermentas, Germany). As shown in Figure 8, the PEG-*b*-P[Asp(DET)] catiomer showed > 20-fold higher 50% growth-inhibitory concentration (IC_{50}) than BPEI and LPEI, highlighting the remarkably low cytotoxicity of the block catiomers synthesized in this study.

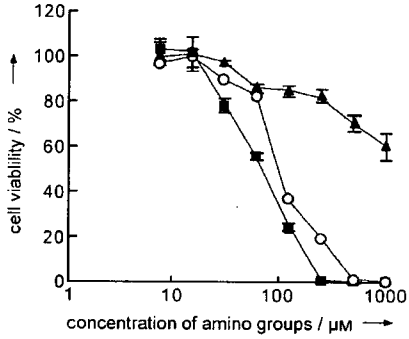

Figure 8. Cytotoxicity of branched (BPEI, ○) and linear (LPEI, ■) polyethylenimines and PEG-*b*-P[Asp(DET)] (▲) against HuH-7 cells. The cells were incubated with each catiomer with different concentrations for 48 h.

The major challenge for the practical use of synthetic vectors in gene therapy is the effective and non-cytotoxic gene transfer to primary cells with therapeutic interest. To evaluate the feasibility of the PEG-*b*-P[Asp(DET)] polyplex micelles toward such primary cells, mouse primary osteoblasts, which are the focus of clinical interest in bone regeneration,[16] were challenged with the polyplex micelles. The luciferase plasmid was transfected, and the resulting TE and cytotoxicity profiles are shown in Figure 9. Notably, the PEG-*b*-P[Asp(DET)] system with $N/P = 80$ gave a TE similar to the polyplexes from ExGen500, the most effective transfection reagent based on LPEI,[17] with the optimal *N/P* ratios (Figure 9A). Nonetheless, the PEG-*b*-P[Asp(DET)] system exhibited no appreciable cytotoxicity under the conditions of gene transfection (Figure 9B).

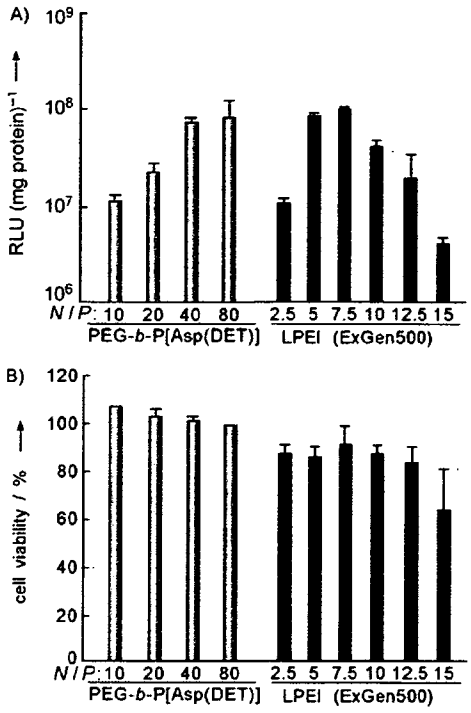

Figure 9. A) In vitro transfection efficiency and B) cytotoxicity of the PEG-*b*-P[Asp(DET)] polyplex micelles and LPEI polyplexes with varying *N/P* ratios toward mouse primary osteoblasts after a 48 h incubation.

Thus, we have successfully obtained highly transfection-efficient and less toxic polyplex micelles in this study. Particularly, the less toxic nature of the block catiomers compared with conventional catiomers of high transfection efficiency, as observed in Figure 8, should be of great significance for in vivo nonviral gene therapy. Indeed, bone regeneration in critical-size cranial defects based on in vivo transduction of osteogenic factors was recently carried out by our research group by using the PEG-*b*-P[Asp(DET)] polyplex micelle with plasmids expressing the optimized combination of osteogenic factors to facilitate cellular differentiation in situ.[18] Furthermore, polyplex micelles with the PEG palisade seem to be suitable for systemic gene delivery,[7,11] and the engineering the constituent block catiomers to construct polyplex micelles with integrated smart functions such as environment sensitivity[8,10] and tissue targetability[9] will maximize the efficacy of nonviral gene therapy. Thus, the PEG-*b*-P[Asp(DET)] polyplex micelle is expected to be a biocompatible vector system applicable toward various aspects of gene medicine.

Conclusion

We have established a simple and novel synthetic route for the generation of biocompatible block catiomers through the quantitative aminolysis of PEG-*b*-PBLA. The construction of a library of block catiomers, the PEG-*b*-polyaspartamides carrying a series of amine compounds in the side chain, revealed the importance of the ethylenediamine unit for enhanced and less toxic gene transfection by the polyplex micelles made from pDNA and the block catiomers. The availability of the polyplex micelles developed in this study for the transfection of primary osteoblasts will facilitate the use of this type of block catiomer for the construction of synthetic vectors suitable for nonviral gene therapy.

Experimental Section

Materials: β-Benzyl-L-aspartate *N*-carboxyanhydride (BLA-NCA) and α-methoxy-ω-amino poly(ethylene glycol) (MeO-PEG-NH_2) (M_r = 12000) were obtained from Nippon Oil and Fats (Tokyo, Japan). Ethylenediamine (EDA), diethylenetriamine (DET) and 4-methyldiethylenetriamine (MDET) were purchased from Tokyo Kasei Kogyo (Tokyo, Japan) and distilled over CaH_2 under decreased pressure. *N,N*-Diethyldiethylenetriamine (DEDET) was purchased from Lancaster Synthesis, (Lancashire, England) and distilled over CaH_2 under decreased pressure. *N,N*-Dimethylformamide (DMF), dichloromethane, and acetic anhydride were purchased from Wako Pure Chemical Industries, (Osaka, Japan) and purified by general methods before use.

Synthesis of PEG-*b*-polyaspartamide catiomers: The PEG-*block*-poly(β-benzyl L-aspartate) (PEG-*b*-PBLA) copolymer was prepared as previously reported.[19] Briefly, BLA-NCA was polymerized in DMF at 40 °C by the initiation from the terminal primary amino group of MeO-PEG-NH_2, followed by acetylation of the *N*-terminus of PBLA to obtain PEG-*b*-PBLA. PEG-*b*-PBLA was confirmed to have a unimodal molecular weight distribution (M_w/M_n: 1.17) by gel-permeation chromatography (GPC) measurement (columns: TSK-gel G4000HHR + G3000HHR, eluent: DMF + 10 mM LiCl, T = 40 °C, detector: RI) (data not shown). The degree of polymerization (DP) of PBLA was calculated to be 68 based on ^{1}H NMR spectroscopy (data not shown).

Lyophilized PEG-*b*-PBLA (300 mg, 11.6 μmol) was dissolved in DMF (10 mL), followed by reaction with DET (50 equiv to benzyl group of PBLA segment, 4.0 g, 39.4 mmol) under mild anhydrous conditions at 40 °C to obtain PEG-*b*-P[Asp(DET)]. After 24 h, the reaction mixture was slowly added dropwise into a solution of acetic acid (10% *v/v*, 40 mL) and dialyzed against a solution of 0.01 N HCl and distilled water (*M*, cutoff: 3500 Da). The final solution was lyophilized to obtain the polymer as the chloride salt form, and the yield was approximately 90%. Similarly, other block catiomers, PEG-*b*-P[Asp(EDA)], PEG-*b*-P[Asp(MDET)], and PEG-*b*-P[Asp(DEDET)] were synthesized by the aminolysis reaction of PEG-*b*-PBLA with EDA, MDET, and DEDET, respectively. The structures of these block catiomers were confirmed by ^{1}H and ^{13}C NMR measurements and size-exclusion chromatography (SEC).

Potentiometric titration of block catiomers: PEG-*b*-P[Asp(DET)] (30 mg) was dissolved in 50 mL 0.01 N HCl and titrated with 0.01 N NaOH. An automatic titrator (TS-2000, Hiranuma, Kyoto, Japan) was used for titration. In this experiment, the titrant was added in quantities of 0.063 mL after the pH values were stabilized (minimal interval: 30 s). The α/pH curves were determined from the obtained titration curves.

Dye exclusion assay: Polyplex solutions with a pDNA concentration of 33 μg mL^{-1}, prepared by mixing pDNA and block catiomers at different *N/P* ratios (N = total amines in block catiomer; P = total phosphate anions in pDNA), were diluted to 10 μg pDNA mL^{-1} with ethidium bromide (EtBr, 2.5 mg mL^{-1}) in 10 mM Tris-HCl (pH 7.4) or 10 mM sodium acetate (pH 5.0) buffer. The sample solutions were incubated at ambient temperature overnight. The fluo-

rescence intensity of the samples at $\lambda = 590$ nm (excitation at $\lambda = 510$ nm) was measured at 25 °C with a spectrofluorometer (FP-6500, Jasco, Tokyo, Japan). The relative fluorescence intensity was calculated as: $F_r = (F_{sample} - F_0)/(F_{100} - F_0)$, for which F_{sample}, F_{100}, and F_0 represent the fluorescence intensity of the samples, free pDNA, and background, respectively.

Dynamic light scattering (DLS) and ζ potential measurements: In the DLS measurements, polyplex solutions with various *N/P* ratios in 10 mM Tris–HCl buffer (pH 7.4) were adjusted to have pDNA concentrations of 33.3 $\mu g\,mL^{-1}$. DLS measurements were then performed at 25 ± 0.2 °C with a DLS-7000 instrument (Otsuka Electronics, Osaka, Japan) with a vertically polarized incident beam of $\lambda = 488$ nm from an Ar ion laser. The ζ potential of the polyplex micelles was measured at 25 ± 0.2 °C with an ELS-6000 instrument (Otsuka Electronics, Osaka, Japan) equipped with a He–Ne ion laser ($\lambda = 633$ nm). The scattering angle was fixed at 20°. From the obtained electrophoretic mobility, the ζ potential was calculated by using the Smoluchowski equation: $\zeta = 4\pi\eta\upsilon/\varepsilon$ in which η is the electrophoretic mobility, υ is the viscosity of the solvent, and ε is the dielectric constant of the solvent. The results are expressed as the average of five experiments.

In vitro transfection of HuH-7 cells: Human hepatoma HuH-7 cells were seeded on 6-well culture plates and incubated overnight in 1.5 mL Dulbecco's modified Eagle medium (DMEM) containing 10% fetal bovine serum (FBS) before transfection. The cells were then incubated with the polyplex micelles from PEG-*b*-P[Asp(EDA)], PEG-*b*-P[Asp(DET)], PEG-*b*-P[Asp(MDET)], and PEG-*b*-P[Asp(DEDET)] (3 μg pDNA/well) with various *N/P* ratios in DMEM containing 10% FBS for 24 h, followed by an additional incubation for 24 h in the absence of polyplexes. Luciferase gene expression was evaluated using the Luciferase Assay System (Promega, Madison, USA) and a Lumat LB9507 luminometer (Berthold Technologies, Bad Wildbad, Germany). The results were expressed as light units per milligram of cell protein determined by a BCA assay kit (Pierce, Rockford, USA).

Mouse primary osteoblast culture and transfection: Osteoblasts were isolated from calvariae of neonatal littermates. The experimental procedures were handled in accordance with the guidelines of the Animal Committee of the University of Tokyo. Calvariae were digested for 10 min at 37 °C in an enzyme solution containing 0.1% collagenase and 0.2% dispase for five cycles. Cells isolated by the final four digestions were combined as an osteoblast population and cultured in DMEM containing 10% FBS. For luciferase transfection assays, primary osteoblasts were inoculated at a density of 2×10^4 cells/well in a 24-multiwell plate, cultured for 24 h, and, after changing to fresh culture medium containing 10% FBS, pDNA polyplex solution (33.3 $\mu g\,mL^{-1}$, 22.5 μL) was applied to each well. Luciferase gene expression was measured 48 h later by using the Luciferase Assay System (Promega) and a Lumat LB9507 luminometer (Berthold). For the cytotoxicity assay, primary osteoblasts were plated into a 96-multiwell plate (6×10^3 cells/well). After 24 h incubation, 6 μL of each pDNA polyplex solution was added, followed by further incubation for 24 h. The viability of the cells was evaluated by an MTT assay (Cell Counting Kit-8, Dojindo, MTT = 3-[4,5-dimethylthiazol-2-yl]-2,5-diphenyltetrazolium bromide). Each well was measured by reading the absorbance at $\lambda = 450$ nm according to the protocol provided by the manufacturer.

Acknowledgements

The authors are grateful to the Health and Labor Sciences Research Grants in Research on Advanced Medical Technology in Nanomedicine Area from the Ministry of Health, Labor and Welfare (MHLW), Japan. They also express their thanks for the Grant-in-Aid for Scientific Research, the Special Coordination Funds for Promoting Science and Technology, and the Project on the Materials Development for Innovative Nano-Drug Delivery Systems from the Ministry of Education, Culture, Sports, Science and Technology (MEXT), Japan. The authors thank Professor Yukio Nagasaki and Dr. Motoi Oishi (University of Tsukuba) for use of the SEC instruments and their helpful suggestions, and Mr. Masataka Nakanishi for valuable discussions.

Keywords: aminolysis · block copolymers · gene delivery · polycations · polymeric micelles

[1] I. M. Verma, N. Somia, *Nature* **1997**, *389*, 239.
[2] M. Ogris, E. Wagner, *Drug Discovery Today* **2002**, *7*, 479.
[3] A. K. Salem, P. C. Searson, K. W. Leong, *Nat. Mater.* **2003**, *2*, 668.
[4] N. Nishiyama, A. Iriyama, W.-D. Jang, K. Miyata, K. Itaka, Y. Inoue, H. Takahashi, Y. Yanagi, Y. Tamaki, H. Koyama, K. Kataoka, *Nat. Mater.* **2005**, *4*, 934.
[5] S. O. Han, R. I. Mahato, S. W. Kim, *Bioconjugate Chem.* **2001**, *12*, 337.
[6] Y. Liu, L. Wenning, M. Lynch, T. M. Reineke, *J. Am. Chem. Soc.* **2004**, *126*, 7422.
[7] K. Itaka, K. Yamauchi, A. Harada, K. Nakamura, H. Kawaguchi, K. Kataoka, *Biomaterials* **2003**, *24*, 4495.
[8] K. Miyata, Y. Kakizawa, N. Nishiyama, A. Harada, Y. Yamasaki, H. Koyama, K. Kataoka, *J. Am. Chem. Soc.* **2004**, *126*, 2355.
[9] D. Wakebayashi, N. Nishiyama, Y. Yamasaki, K. Itaka, N. Kanayama, A. Harada, Y. Nagasaki, K. Kataoka, *J. Controlled Release* **2004**, *95*, 653.
[10] S. Fukushima, K. Miyata, N. Nishiyama, N. Kanayama, Y. Yamasaki, K. Kataoka, *J. Am. Chem. Soc.* **2005**, *127*, 2810.
[11] M. Harada-Shiba, K. Yamauchi, A. Harada, I. Takamisawa, K. Shimokado, K. Kataoka, *Gene Ther.* **2002**, *9*, 407.
[12] Y.-Y. Kim, H.-C. Chang, Y. T. Lee, U.-I. Cho, D. W. Boo, *J. Phys. Chem. A* **2003**, *107*, 5007.
[13] J.-P. Behr, *Chemia* **1997**, *51*, 34.
[14] V. Saudek, H. Pivcova, J. Drobnik, *Biopolymers* **1981**, *20*, 1615.
[15] A. V. Kabanov, T. K. Bronich, V. A. Kabanov, K. Yu, A. Eisenberg, *Macromolecules* **1996**, *29*, 6797.
[16] R. T. Franceschi, S. Yang, R. B. Rutherford, P. H. Krebsbach, M. Zhao, D. Wang, *Cells Tissues Organs* **2004**, *176*, 95–108.
[17] C. L. Gebhart, A. V. Kabanov, *J. Controlled Release* **2001**, *73*, 401.
[18] K. Itaka, N. Kanayama, N. Nishiyama, S. Fukushima, Y. Yamasaki, S. Oba, U.-I. Chung, H. Kawaguchi, K. Nakamura, K. Kataoka, *Proceedings of the 12th International Symposium on Recent Advances in Drug-Delivery Systems and CRS Winter Symposium, Salt Lake City, Utah, USA, February 21–24*, **2005**, 9.
[19] A. Harada, K. Kataoka, *Macromolecules* **1995**, *28*, 5294.

Received: December 21, 2005
Published online on February 24, 2006

CLINICAL ORTHOPAEDICS AND RELATED RESEARCH
Number 453, pp. 58–63

2006 FRANK STINCHFIELD AWARD

Grafting of Biocompatible Polymer for Longevity of Artificial Hip Joints

Toru Moro, MD; Yoshio Takatori, MD*; Kazuhiko Ishihara, PhD†; Kozo Nakamura, MD*; and Hiroshi Kawaguchi, MD**

Aseptic loosening induced by wear particles from the polyethylene liner is likely the most common cause of long-term total hip arthroplasty failure. We developed a novel hip polyethylene liner with the surface graft of a biocompatible phospholipid polymer, 2-methacryloyloxyethyl phosphorylcholine (MPC), and previously reported the grafting decreased the short-term production of wear particles and the subsequent bone resorptive responses. For clinical application, we investigated the stability of the 2-methacryloyloxyethyl phosphorylcholine grafting during sterilization and the wear resistance of the sterilized liner during longer loading comparable to clinical usage. Radiographic spectroscopy confirmed the stability of the 2-methacryloyloxyethyl phosphorylcholine polymer on the liner surface after the gamma irradiation. We used a hip wear simulator up to 1×10^7 cycles to test sterilized cross-linked polyethylene liners with and without 2-methacryloyloxyethyl phosphorylcholine grafting. The 2-methacryloyloxyethyl phosphorylcholine grafting markedly decreased the friction, the production of wear particles, and the wear of the liner surface. These data suggest a marked improvement in the wear resistance of the polyethylene liner by the 2-methacryloyloxyethyl phosphorylcholine grafting for clinically relevant periods after sterilization, indicating 2-methacryloyloxyethyl phosphorylcholine grafting is a promising technology for extending longevity of artificial hips.

From the *Department of Sensory & Motor System Medicine, Faculty of Medicine; and the †Department of Materials Engineering, School of Engineering, The University of Tokyo, Tokyo, Japan.
One or more of the authors has received funding from grants-in-Aid for Scientific Research from the Japanese Ministry of Education, Culture, Sports, Science and Technology (#15390449) (YT), and Health and Welfare Research Grant for Translational Research from the Japanese Ministry of Health, Labour and Welfare (KN).
Correspondence to: Toru Moro, MD, PhD, Department of Sensory & Motor System Medicine, Faculty of Medicine, The University of Tokyo, Hongo 7-3-1, Bunkyo, Tokyo 113-0033, Japan. Phone: 81-3-5800-8656; Fax: 81-3-3818-4082; E-mail: moro-ort@h.u-tokyo.ac.jp.
DOI: 10.1097/01.blo.0000246553.33434.5f

The incidence of osteoarthritis (OA) is on the rise because of the worldwide growth of elderly populations. Total hip arthroplasty (THA) is one of the most successful and effective treatments for patients with end-stage arthritic diseases of the hip.[4,37] The number of primary THAs performed annually is estimated to be more than 1.3 million worldwide, with 50 to 140 operations per 100,000 inhabitants in North America, Europe, and Australia. This rate is expected to continue to increase over at least the next three decades.[1,25,33] Despite improvements in implant design and surgical technique, aseptic loosening of artificial joints caused by periprosthetic osteolysis is the most common problem limiting implant survivorship and clinical success.[21] However, there is no treatment for painful loosening other than the revision surgery, and the number of salvage operations with outcomes poorer than the primary procedures is increasing.[29]

The pathogenesis of the periprosthetic osteolysis is a consequence of the host inflammatory response to wear particles from prosthetic devices.[21] The most abundant and bone resorptive particle within the periprosthetic tissue is polyethylene (PE) generated from the interface between PE and metal components.[30] Polyethylene particles induce phagocytosis by macrophages and subsequently secretion of bone resorptive cytokines.[9] Therefore, there are two approaches to prevent aseptic loosening: reduce the amount of PE wear particles or suppress the subsequent bone resorptive responses. Studies have been performed to increase the wear resistance of PE or to develop alternative bearing surfaces other than PE, but none has fully solved the problem.

The surface of healthy human articular cartilage is covered with a nanometer-scaled phospholipid layer that improves the lubricity and biocompatibility of the articulating surface.[13,24] Therefore, grafting a polymer including the biocompatible phospholipid-like layer on an artificial liner surface may replicate interface conditions similar to a healthy joint. The 2-methacryloyloxyethyl phosphoryl-

choline (MPC) polymer, the natural biocompatible polymer, has a side chain composed of phosphorylcholine resembling phospholipids of biomembrane (Fig 1).[20] The MPC grafting onto the surface of other medical devices suppresses biological reactions when they are in contact with living organisms,[19,42] and is now clinically used on the surfaces of intravascular stents, intravascular guide wires, soft contact lenses, and the artificial lung authorized by the United States Food and Drug Administration.[23,27]

To reduce wear particles and eliminate periprosthetic osteolysis, we prepared a novel PE hip liner with MPC grafted onto its surface. Our previous study suggests grafted MPC decreases the production of wear particles and secretion of cytokines and osteoclastogenesis during a brief period of 3×10^6 cycles in a hip wear simulator.[34] However, the effect of the sterilization procedure on the stability of the MPC grafting and the wear resistance of the sterilized liner during longer loading comparable to clinical usage remains to be elucidated before clinical application.

We evaluated MPC stability after sterilization and the wear resistance of the sterilized MPC-grafted PE liner during longer loading comparable to clinical usage.

MATERIALS AND METHODS

We used a hip simulator to investigate the MPC stability after sterilization and the wear resistance of the sterilized MPC-grafted PE liner during 1×10^7 cycles of loading, comparable to 10 to 30 years of walking. The stability of the MPC polymer on MPC-CLPE plate after the gamma irradiation was verified using the xray photoelectron spectroscopy (XPS) analysis, the Fourier transform infrared spectroscopic (FTIR) analysis, and the contact angle of a water drop. Mechanical effects of the MPC grafting on the hip prosthesis were examined using a hip wear simulator[22] under the conditions recommended by the International Organization for Standardization.

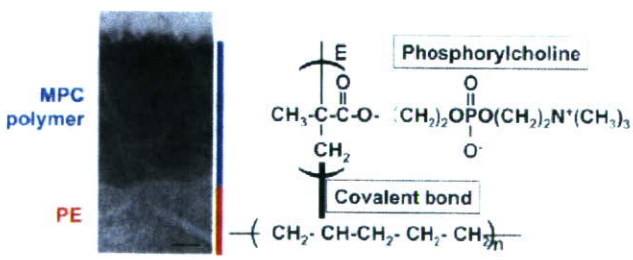

Fig 1. The MPC polymer is grafted onto the cross-linked polyethylene liner surface. A TEM image (left) shows the cross-linked PE liner surface grafted with MPC polymer stained black with ruthenium oxide show (scale bar, 20 nm). The chemical structure (right) of MPC and cross-linked PE is shown. 2-methacryloyloxyethyl phosphorylcholine is a biocompatible polymer with side chain composed of phosphorylcholine and resembles phospholipid of biomembrane. MPC is bound to the cross-linked PE liner by the covalent bond with a photoinduced graft polymerization technique.

We synthesized and purified MPC as previously reported (Fig 1).[20] We used cross-linked PE liner (K-MAX Excellink®, Japan Medical Materials, Osaka, Japan) and cobalt-chromium-molybdenum alloy femoral heads (K-MAX® HH-02, Japan Medical Materials). Grafting of the MPC polymer onto the surfaces of the cross-linked PE liner was performed using a photo-induced polymerization technique.[16,34] Briefly, cross-linked PE liners were placed in the MPC solution (0.5 mol/L) and photo-induced polymerization on the liner surface was performed using an ultra-high pressure mercury lamp (UVL-400HA, Riko-Kagaku Sangyo Co Ltd, Chiba, Japan).

To evaluate the influence of sterilization procedure, MPC-grafted cross-linked PE plates (MPC-CLPE plates) were sterilized with gamma irradiation (2.5 Mrad) in nitrogen as conventionally used. Elemental analysis at the surface was performed with a highly sensitive XPS (PHI5400MC, Perkin Elmer, Inc, Wellesley, MA), a FTIR (Perkin-Elmer FT-IR 1650, Perkin Elmer, Inc), and a transmission electron microscope (JEM-1010 Japan Electron Optics Laboratory Co, Ltd, Tokyo, Japan). The contact angle of water on the cross-linked PE surface was measured by the sessile drop method at room temperature (22°C) using a goniometer (Erma G-1, Tokyo, Japan).[18] At least 10 contact angles were measured and averaged.

A 12-station hip simulator apparatus (MTS, MTS Systems Co Ltd, Minneapolis, MN) with two types of gamma-sterilized cross-linked PE liners in 46 mm acetabular cups, a cross-linked PE liner and an MPC-grafted cross-linked PE liner (MPC-CLPE liner), coupled to 26 mm cobalt-chromium-molybdenum alloy heads were mounted on the rotating blocks to produce a biaxial or orbital motion. Friction torque between the liner and the femoral head was measured using a torque measuring instrument. We then applied a loading profile that simulated walking with continuous cyclic motion and loading (maximum force, 2744 N; frequency, 1 Hz).[38] A diluted bovine calf serum (25%) in distilled water was used as the lubricant. Sodium azide (10 mL/L) and ethylenediaminetetraacetic acid (20 mm) were added to prevent microbial contamination and minimize calcium phosphate formation on the implant surface. The simulator was run up to 1×10^7 cycles for 8 months. At intervals of 5×10^5 cycles the liners were removed from the simulator and weighed on a microbalance (Sartorius GENIUS ME215S, Sartorius AG, Göttingen, Germany). The lubricant was collected and stored at −20°C for further analysis. After total loading, microdamage of the liner surface was measured with a three-dimensional coordinate measuring machine (XYZAX GS800B, Tokyo Seimitsu Co, Ltd, Tokyo, Japan). To evaluate true removal of material caused by wear, melt-recovery experiments were performed and the liner surface was analyzed with confocal scanning laser microscope (OLS1200, Olympus Corp, Tokyo, Japan) as previously reported.[35] For the femoral head surface, in addition to scanning electron microscopy (SEM) evaluation, the surface roughness value R_a was measured using a roughness measuring instrument (SURFTEST-501, Mitsutoyo Co, Ltd, Kanagawa, Japan) with a 5 μm diameter contact probe. For the isolation of wear particles after loading, the lubricant was incubated with 5 N NaOH solu-

tion to digest adhesive proteins that were degraded and precipitated. Collected particles underwent sequential filtrations as previously reported.[22] The size of particles was defined as the maximum dimensions by the SEM analysis.

We compared the means of CLPE and MPC-CLPE groups by analysis of variance and determined significance by post-hoc testing using Bonferroni's method.

RESULTS

The XPS signals indicating nitrogen atoms (N_{1s}) at 402 eV and phosphorus atoms (P_{2p}) at 135 eV, which are attributable to the phosphorylcholine group in the MPC unit, were observed on the MPC-CLPE plate after gamma irritation (Fig 2A). The FTIR transmittance absorption representing phosphate group (P-O) at 1240, 1080, and 970 cm^{-1}, and ketone group (C = O) at 1720 cm^{-1} also was observed after grafting and irradiation (Fig 2B). The contact angle of a water droplet on the MPC-CLPE plate was 12.3° ± 2.4°, whereas the contact angle of a water droplet of the original cross-linked PE plate was 89.9° ± 2.9° (Fig 2C), suggesting the hydrophobic cross-linked PE surface was kept covered with hydrophilic MPC polymer after the gamma irritation.

In the hip simulator study (Fig 3A) the average friction torque was approximately 80% lower in MPC-CLPE liners than in cross-linked PE liners (Fig 3B). The gravimetric analysis showed a total weight loss of 34.7 ± 2.5 mg in cross-linked PE liners after 1×10^7 cycles of loading (Fig 3C). In contrast, MPC-CLPE liners continued to gain weight, showing a total weight gain of 8.7 ± 1 mg, which may have been attributable to water absorption into the liner from the lubricant.

Three-dimensional morphometric analyses of MPC-CLPE liner surface revealed little or no detectable wear, while substantial wear was detected in cross-linked PE liners (Fig 4A). The confocal scanning laser microscopic analysis of the liner surface clearly revealed original machine marks on the MPC-CLPE liner surface, but they were completely obliterated from the cross-linked PE liner (Fig 4B). The XPS analysis also confirmed the remainder of the specific spectra of N_{1s} and P_{2p} on the MPC-CLPE liner surface after the loading (Fig 2A), indicating the MPC-CLPE grafting was maintained after loading 1×10^7 cycles. The femoral heads were free of visible scratches and the surface roughness expressed by the R_a values was similar before and after loading in both groups (R_a = 0.04 – 0.05 μm), suggesting there was no abrasive contamination with metal particles from the heads in the hip simulator (Fig 4C).

The SEM analysis of the wear particles isolated from the lubricants showed no difference in the particle shapes or sizes between cross-linked PE and MPC-CLPE liners. Most of the particles from both liners ranged from 0.1 μm to1 μm and were round or spindle-shaped (Fig 5).

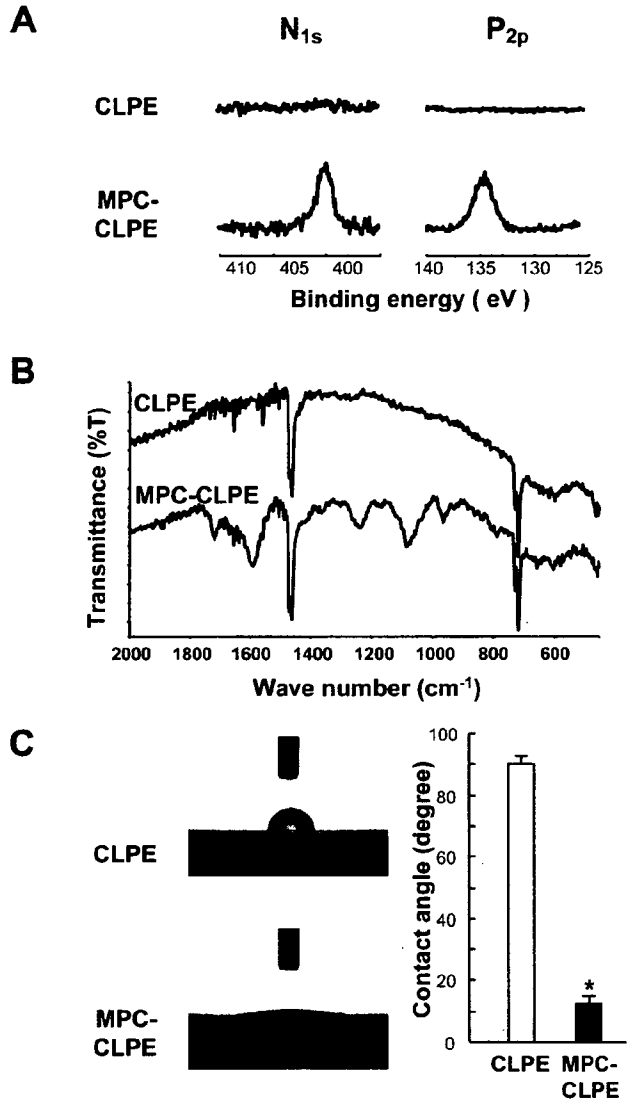

Fig 2A–C. (A) Xray photoelectron spectra of the cross-linked PE and MPC-CLPE plates after gamma sterilization are shown. The peaks in the nitrogen (N1s) and phosphorus (P2p) atom regions are specific to MPC, suggesting gamma sterilization did not affect the properties of MPC grafting. (B) Fourier transform infrared spectra of the cross-linked PE and MPC-CLPE plates after gamma sterilization are shown. Absorptions representing the phosphate group (P–O) at 1240, 1080, and 970 cm^{-1}, and ketone group (C = O) at 1720 cm^{-1} are also specific to MPC. (C) Hydrophilicity determined by the contact angle of a water drop with the cross-linked PE and MPC-CLPE plates after gamma sterilization is represented. Data are expressed as means (bars) ± standard errors (error bars) for 12 plates per group (*significant difference from cross-linked PE was set at $p < 0.01$).

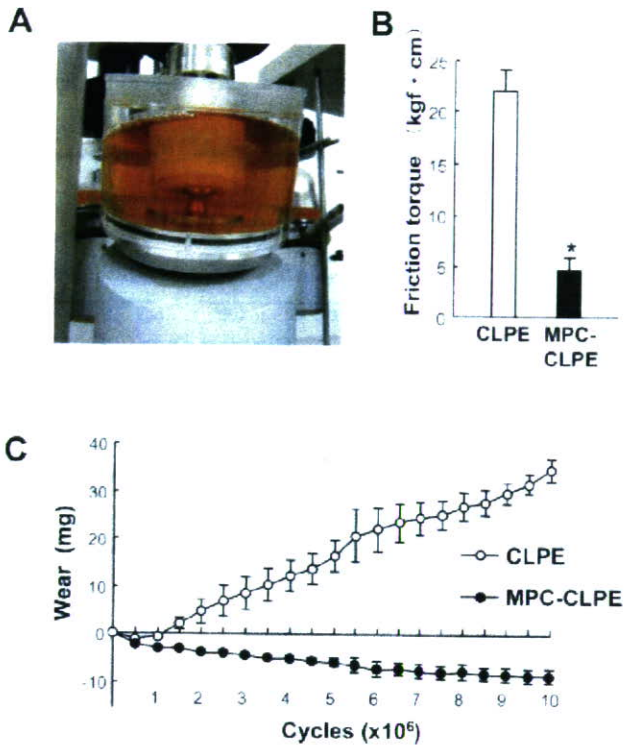

Fig 3A–C. (A) A photograph shows the hip simulator. (B) The bar graph shows friction torque of the cross-linked PE and MPC-CLPE liners against the femoral heads measured before the loading test. (C) The graph shows the time course of the amount of wear product from cross-linked PE and MPC-CLPE liners during 1×10^7 cycles of loading. Data are expressed as means (symbols and bars) ± standard errors (error bars) for 10 liners/group (*significant difference from cross-linked PE was set at $p < 0.01$).

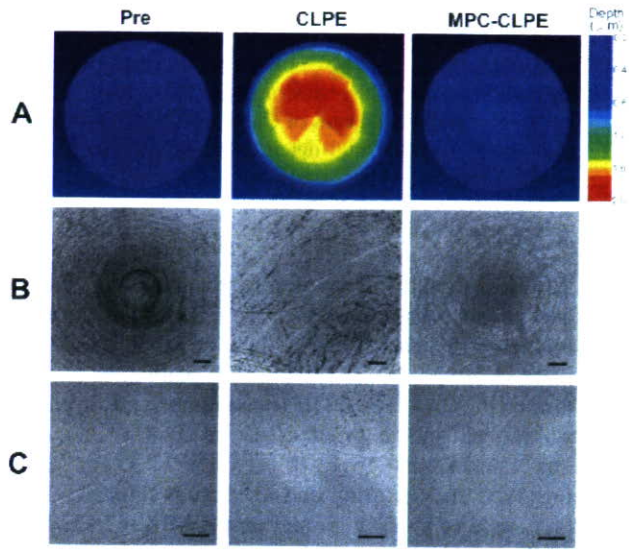

Fig 4A–C. (A) Three-dimensional morphometric analysis and (B) confocal scanning laser microscopic analysis of the liner surfaces before (pre) and after 1×10^7 cycles of loading on cross-linked PE and MPC-CLPE liners is shown (scale bars, 200 μm). (C) Scanning electron microscopy analyses of the femoral head surfaces before (pre) and after 1×10^7 cycles of loading showed the femoral heads were free of visible scratches in both liners (scale bars, 5 μm).

DISCUSSION

Our data suggest the biocompatible phospholipid polymer MPC grafted onto the PE liner surface of the hip prosthesis decreases friction and the production of wear particles during 1×10^7 cycles of loading in a hip simulator. Because PE particles are the most abundant and catabolic among wear particles in the periprosthetic tissues,[30] alternative bearing surfaces have been proposed such as ceramic-on-ceramic and metal-on-metal articulations; however, these have potential disadvantages.[2,3]

The major limitation of our study is the confined period of loading. Although the 1×10^7 cycles in the hip simulator is comparable to 10 to 30 years of physical walking, this may not be long enough for young active patients with aseptic necrosis or fracture. A hip simulator study with longer loading is now underway. Furthermore, a hip simulator does not entirely capture the range of loading conditions of a hip, in terms of either the variety of positions or the magnitude of loading. Nonetheless, we believe a simulator study can provide some indication of trends.

The long history and popularity of PE as a bearing surface has led to research in the development of tougher

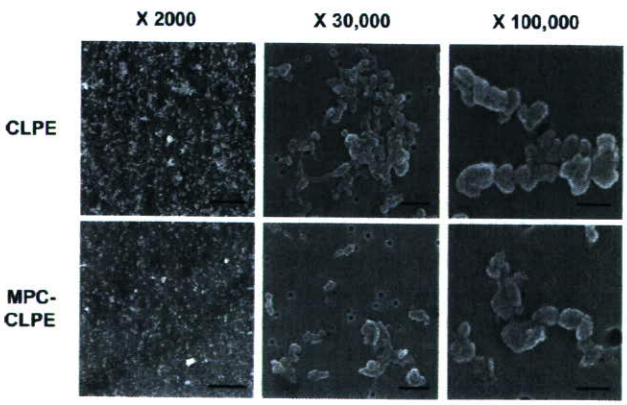

Fig 5. Scanning electron microscopy images show the wear particles isolated from lubricants of the simulators with cross-linked PE and MPC liners. Representative images are shown in three magnifications (×2000, ×30,000, and ×100,000; scale bars, 10 μm, 500 nm, and 200 nm, respectively).

and more wear-resistant PE materials. These include the incorporation of short chopped carbon fibers in PE matrix,[6,41] the extension of chain crystallite morphology with thicker lamellae and higher crystallinity,[28] and the creation of a three-dimensional molecular network by cross-linking. Of these, cross-linking improved the wear resistance and suppressed the periprosthetic osteolysis most efficiently in the clinical setting.[31] Grafting of MPC onto the cross-linked PE surface further increased the wear resistance over the conventional cross-linked PE.

Clinical and laboratory research suggests sterilization methods can dramatically affect the in vivo performance of PE liners.[32] Currently, PE liners can be sterilized with gamma irradiation, gas plasma, or ethylene oxide. Gamma sterilization in air has been shown to lead to oxidation of the PE and may adversely affect its mechanical properties. In the mid-1990s, the use of gamma sterilization in air was replaced by gamma sterilization in an inert environment, such as nitrogen, argon, or a vacuum. We used cross-linked PE liners sterilized gamma irradiation in nitrogen, and our data suggest this sterilization method did not affect the property of MPC grafting with respect to surface analysis and hip simulator study. Other MPC-grafted medical devices such as an oxygenator, intravascular stents, or intravascular guide wires are sterilized with gamma irradiation or ethylene oxide. Moreover, the MPC polymer has good thermal resistance and could be processed by heat treatment at 150°C. Our preliminary study showed gas plasma and ethylene oxide sterilization did not affect properties of the MPC polymer.[36]

Given a reduction of wear by the MPC grafting, we should consider the lubrication mechanism between the liners and metal heads. Although phospholipids work as effective boundary lubricants,[12,40] a study of natural synovial joints showed fluid film lubrication by the intermediate hydrated layer is the predominant mechanism under physiologic walking conditions.[7] Because we showed the MPC grafting onto the cross-linked PE plate increased hydrophilicity, and our previous study showed the free water fraction on the MPC polymer surface is kept at a higher level,[17] the reduction of wear is likely attributable to the hydrated lubricating layer formed by MPC grafting.

In addition to the improvement of the wear resistance of the liner, it is important to decrease bone resorptive responses induced by wear particles. Substantial differences between the wear particles from cross-linked and non-cross-linked PE liners have been found in vitro.[8,15] The cross-linked PE liner releases a relatively high number of submicrometer and nanometer-sized PE particles and relatively fewer particles that are several micrometers in dimension.[11] These submicrometer-sized PE particles induce a greater inflammatory response in vitro than larger particles.[15] Therefore, the biological activity of PE particles will depend on the total volume of wear or the number of particles generated and the proportion of those particles that are within the most biologically active size range.[8,11] In our previous study, MPC nanoparticles (500 nm in diameter) were used in a murine particle-induced osteolysis model to investigate the biocompatibility of these particles.[34] In vitro culture systems suggested MPC nanoparticles were not phagocytosed in substantial amounts by macrophages and do not induce the production of bone resorptive cytokines. Furthermore, the culture medium of macrophages exposed to MPC nanoparticles did not induce osteoclast formation from bone marrow cells. These results suggest MPC particles are biologically inert in respect to phagocytosis by macrophages and subsequent bone resorptive actions. An increasing number of studies address the potential pharmacologic modification of the adverse host response to wear particles,[5,10] including cytokine antagonists, cyclooxygenase-2 inhibitors, and osteoprotegerin, or anti-RANKL (receptor activator of nuclear vector kappa B ligand) antibody; however, they may cause serious side effects because the agents must taken for a long period after surgery and because they are not currently targeted to the site of the problem. Because the lack of side effects of the MPC polymer grafting has already been confirmed clinically by several biomaterials,[23,26] this grafting surpasses the developing pharmacologic treatments.

Although our study focused on the hip, MPC polymer grafting can be applicable to the prevention of periprosthetic osteolysis of other joints in which PE particles from articular interfaces between the PE and metal components are also thought to initiate the catabolic cascade.[14,39] From the advantages observed, we believe MPC polymer grafting will improve total joint replacement by preventing periprosthetic osteolysis and aseptic loosening. The development of this nanotechnology would improve the quality of care of patients having total joint replacement and have a substantial public health impact. We are currently designing a large-scale clinical trial.

Acknowledgments

We thank Tomohiro Konno, Noboru Yamawaki, Takatoshi Miyashita, Masayuki Kyomoto, Hiroaki Takadama, Kaori Jono, and Reiko Yamaguchi for their excellent technical help.

References

1. Birrell F, Johnell O, Silman A. Projecting the need for hip replacement over the next three decades: influence of changing demography and threshold for surgery. *Ann Rheum Dis*. 1999;58:569–572.
2. Black J. Metal on metal bearings. A practical alternative to metal on polyethylene total joints? *Clin Orthop Relat Res*. 1996;329: S244–S255.
3. Callaway GH, Flynn W, Ranawat CS, Sculco TP. Fracture of the femoral head after ceramic-on-polyethylene total hip arthroplasty. *J Arthroplasty*. 1995;10:855–859.

4. Charnley J. Total hip replacement by low-friction arthroplasty. *Clin Orthop Relat Res.* 1970;72:7–21.
5. Childs LM, Paschalis EP, Xing L, Dougall WC, Anderson D, Boskey AL, Puzas JE, Rosier RN, O'Keefe RJ, Boyce BF, Schwarz EM. In vivo RANK signaling blockade using the receptor activator of NF-kappaB:Fc effectively prevents and ameliorates wear debris-induced osteolysis via osteoclast depletion without inhibiting osteogenesis. *J Bone Miner Res.* 2002;17:192–199.
6. Connelly GM, Rimnac CM, Wright TM, Hertzberg RW, Manson JA. Fatigue crack propagation behavior of ultrahigh molecular weight polyethylene. *J Orthop Res.* 1984;2:119–125.
7. Dowson D, Jin ZM. Micro-elastohydrodynamic lubrication of synovial joints. *Eng Med.* 1986;15:63–65.
8. Galvin AL, Tipper JL, Ingham E, Fisher J. Nanometre size wear debris generated from crosslinked and non-crosslinked ultra high molecular weight polyethylene in artificial joints. *Wear.* 2005;259: 977–983.
9. Glant TT, Jacobs JJ, Molnar G, Shanbhag AS, Valyon M, Galante JO. Bone resorption activity of particulate-stimulated macrophages. *J Bone Miner Res.* 1993;8:1071–1079.
10. Goater JJ, O'Keefe RJ, Rosier RN, Puzas JE, Schwarz EM. Efficacy of ex vivo OPG gene therapy in preventing wear debris induced osteolysis. *J Orthop Res.* 2002;20:169–173.
11. Green TR, Fisher J, Stone M, Wroblewski BM, Ingham E. Polyethylene particles of a 'critical size' are necessary for the induction of cytokines by macrophages in vitro. *Biomaterials.* 1998;19: 2297–2302.
12. Hills BA. Boundary lubrication in vivo. *Proc Inst Mech Eng [H].* 2000;214:83–94.
13. Hills BA, Butler BD. Surfactants identified in synovial fluid and their ability to act as boundary lubricants. *Ann Rheum Dis.* 1984; 43:641–648.
14. Inagaki K, O'Driscoll SW, Neale PG, Uchiyama E, Morrey BF, An KN. Importance of a radial head component in Sorbie unlinked total elbow arthroplasty. *Clin Orthop Relat Res.* 2002;400:123–131.
15. Ingram JH, Stone M, Fisher J, Ingham E. The influence of molecular weight, crosslinking and counterface roughness on TNF-alpha production by macrophages in response to ultra high molecular weight polyethylene particles. *Biomaterials.* 2004;25:3511–3522.
16. Ishihara K, Iwasaki Y, Ebihara S, Shindo Y, Nakabayashi N. Photoinduced graft polymerization of 2-methacryloyloxyethyl phosphorylcholine on polyethylene membrane surface for obtaining blood cell adhesion resistance. *Colloids Surf B Biointerfaces.* 2000; 18:325–335.
17. Ishihara K, Nomura H, Mihara T, Kurita K, Iwasaki Y, Nakabayashi N. Why do phospholipid polymers reduce protein adsorption? *J Biomed Mater Res.* 1998;39:323–330.
18. Ishihara K, Okazaki A, Negishi N, Shinohara I, Okano T, Kataoka K, Sakurai Y. Photo-induced change in wettability and binding ability of azoaromatic polymers. *J Appl Polym Sci.* 1982;27: 239–245.
19. Ishihara K, Shinozuka T, Hanazaki Y, Iwasaki Y, Nakabayashi N. Improvement of blood compatibility on cellulose hemodialysis membrane: IV. Phospholipid polymer bonded to the membrane surface. *J Biomater Sci Polym Ed.* 1999;10:271–282.
20. Ishihara K, Ueda T, Nakabayashi N. Preparation of phospholipid polymers and their properties as polymer hydrogel membrane. *Polym J.* 1990;22:355–360.
21. Jacobs JJ, Roebuck KA, Archibeck M, Hallab NJ, Glant TT. Osteolysis: basic science. *Clin Orthop Relat Res.* 2001;393:71–77.
22. Jono K, Takigawa Y, Takadama H, Mizuno M, Nakamura T. A multi-station hip joint simulator study and wear characterization of commercial hip endoprostheses. *Ceram Eng & Sci Proc.* 2003;24: 255–260.
23. Kihara S, Yamazaki K, Litwak KN, Litwak P, Kameneva MV, Ushiyama H, Tokuno T, Borzelleca DC, Umezu M, Tomioka J, Tagusari O, Akimoto T, Koyanag H, Kurosawa H, Kormos RL, Griffith BP. In vivo evaluation of a MPC polymer coated continuous flow left ventricular assist system. *Artif Organs.* 2003;27: 188–192.
24. Kirk TB, Wilson AS, Stachowiak GW. The morphology and composition of the superficial zone of mammalian articular cartilage. *J Orthop Rheumatol.* 1993;6:21–28.
25. Kurtz S, Mowat F, Ong K, Chan N, Lau E, Halpern M. Prevalence of primary and revision total hip and knee arthroplasty in the United States from 1990 through 2002. *J Bone Joint Surg.* 2005;87: 1487–1497.
26. Lewis AL, Furze JD, Small S, Robertson JD, Higgins BJ, Taylor S, Ricci DR. Long-term stability of a coronary stent coating post-implantation. *J Biomed Mater Res.* 2002;63:699–705.
27. Lewis AL, Tolhurst LA, Stratford PW. Analysis of a phosphorylcholine-based polymer coating on a coronary stent pre- and post-implantation. *Biomaterials.* 2002;23:1697–1706.
28. Livingston BJ, Chmell MJ, Spector M, Poss R. Complications of total hip arthroplasty associated with the use of an acetabular component with a Hylamer liner. *J Bone Joint Surg Am.* 1997;79: 1529–1538.
29. Mahomed NN, Barrett JA, Katz JN, Phillips CB, Losina E, Lew RA, Guadagnoli E, Harris WH, Poss R, Baron JA. Rates and outcomes of primary and revision total hip replacement in the United States medicare population. *J Bone Joint Surg Am.* 2003;85:27–32.
30. Maloney WJ, Smith RL, Schmalzried TP, Chiba J, Huene D, Rubash H. Isolation and characterization of wear particles generated in patients who have had failure of a hip arthroplasty without cement. *J Bone Joint Surg Am.* 1995;77:1301–1310.
31. McKellop H, Shen FW, DiMaio W, Lancaster JG. Wear of gamma-crosslinked polyethylene acetabular cups against roughened femoral balls. *Clin Orthop Relat Res.* 1999;369:73–82.
32. McKellop H, Shen FW, Lu B, Campbell P, Salovey R. Effect of sterilization method and other modifications on the wear resistance of acetabular cups made of ultra-high molecular weight polyethylene. A hip-simulator study. *J Bone Joint Surg Am.* 2000;82: 1708–1725.
33. Merx H, Dreinhofer K, Schrader P, Sturmer T, Puhl W, Gunther KP, Brenner H. International variation in hip replacement rates. *Ann Rheum Dis.* 2003;62:222–226.
34. Moro T, Takatori Y, Ishihara K, Konno T, Takigawa Y, Matsushita T, Chung UI, Nakamura K, Kawaguchi H. Surface grafting of artificial joints with a biocompatible polymer for preventing periprosthetic osteolysis. *Nat Mater.* 2004;3:829–836.
35. Muratoglu OK, Greenbaum ES, Bragdon CR, Jasty M, Freiberg AA, Harris WH. Surface analysis of early retrieved acetabular polyethylene liners: a comparison of conventional and highly crosslinked polyethylenes. *J Arthroplasty.* 2004;19:68–77.
36. Ogawa R, Iwasaki Y, Ishihara K. Thermal property and processability of elastomeric polymer alloy composed of segmented polyurethane and phospholipid polymer. *J Biomed Mater Res.* 2002;62: 214–221.
37. Older J. Charnley low-friction arthroplasty: a worldwide retrospective review at 15 to 20 years. *J Arthroplasty.* 2002;17:675–680.
38. Paul JP. Forces transmitted by joints in the human body. *Proc Inst Mech Eng [H].* 1967;181:8–15.
39. Shanbhag AS, Bailey HO, Hwang DS, Cha CW, Eror NG, Rubash HE. Quantitative analysis of ultrahigh molecular weight polyethylene (UHMWPE) wear debris associated with total knee replacements. *J Biomed Mater Res.* 2000;53:100–110.
40. Williams PF 3rd, Powell GL, LaBerge M. Sliding friction analysis of phosphatidylcholine as a boundary lubricant for articular cartilage. *Proc Inst Mech Eng [H].* 1993;207:59–66.
41. Wright TM, Rimnac CM, Faris PM, Bansal M. Analysis of surface damage in retrieved carbon fiber-reinforced and plain polyethylene tibial components from posterior stabilized total knee replacements. *J Bone Joint Surg Am.* 1988;70:1312–1319.
42. Yoneyama T, Sugihara K, Ishihara K, Iwasaki Y, Nakabayashi N. The vascular prosthesis without pseudointima prepared by antithrombogenic phospholipid polymer. *Biomaterials.* 2002;23: 1455–1459.

Eur Spine J (2006) 15: 1521–1528
DOI 10.1007/s00586-005-0005-8

ORIGINAL ARTICLE

Yu Koshizuka
Naoshi Ogata
Masataka Shiraki
Takayuki Hosoi
Atsushi Seichi
Katsushi Takeshita
Kozo Nakamura
Hiroshi Kawaguchi

Distinct association of gene polymorphisms of estrogen receptor and vitamin D receptor with lumbar spondylosis in post-menopausal women

Received: 29 April 2005
Revised: 21 August 2005
Accepted: 9 October 2005
Published online: 14 December 2005

Y. Koshizuka · N. Ogata · A. Seichi
K. Takeshita · K. Nakamura
H. Kawaguchi (✉)
Department of Orthopaedic Surgery,
Faculty of Medicine, University of Tokyo,
Hongo 7-3-1, Bunkyo-ku 113-8655, Tokyo,
Japan
E-mail: kawaguchi-ort@h.u-tokyo.ac.jp
Tel.: +81-3-58008656
Fax: +81-3-38184082

M. Shiraki
Research Institute and Practice
for Involutional Diseases,
Nagano, Japan

T. Hosoi
Tokyo Metropolitan Geriatric Hospital,
Tokyo, Japan

Abstract Contribution of genetic backgrounds to the etiology of lumbar spondylosis has been suggested by epidemiological studies. This study was designed to determine the association of restriction fragment length polymorphisms (RFLPs) of estrogen receptor (ER), vitamin D receptor (VDR), parathyroid hormone (PTH) and interleukin-1β (IL-1β) genes with the radiological severity of lumbar spondylosis at the disk level from L1/2 to L5/S1 in Japanese post-menopausal women. ER and VDR RFLP haplotypes were associated with the severity of spondylosis in the upper levels (L1/2 and L2/3) more than in the lower levels. Association of ER genotype was more pronounced in the group younger than average than in the older group, while that of VDR genotype was more significant in the older group. Neither PTH nor IL1-β RFLP was associated with the severity at any levels in either stratified group. We thus conclude that ER and VDR genes may contribute to lumbar spondylosis in a distinct manner: estrogen sensitivity influences the severity in the early phase after menopause while vitamin D plays an important role at older ages when the contribution of estrogen loss is weaker.

Keywords Spondylosis · Polymorphism · Estrogen receptor · Vitamin D receptor

Introduction

Osteoarthritis including spinal spondylosis, a chronic degenerative joint disorder, is prevalent in society as a major cause of disability. In Western countries, 10–50% of the senior population is affected by osteoarthritis, a quarter of whom are severely disabled due to joint symptoms or neuropathies [6]. In Japan as well, approximately 10 million of the country's 120 million inhabitants are suffering from osteoarthritis, with the figure increasing by 900,000 every year. Because of the prevalence of the disease in the elderly, this trend is occurring worldwide as a consequence of increasing longevity due to the overall improvement in living conditions and health status [21]. Despite significant social demand, research on osteoarthritis is still marginalized within biomedical research, so that the molecular and genetic bases for the disease are largely unmapped.

Family studies have suggested that not only osteoarthritis of the knee and hand [8, 14, 30], but also spinal spondylosis and degeneration [3, 27] have a strong genetic component with an increased prevalence in first-degree relatives of affected individuals. A twin study demonstrated a clear genetic effect for radiographic osteoarthritis of the knee and hand in women, with 39–65% of the variance being explained by genetic factors [30]. Recent population-based case-control studies have disclosed the association of polymorphisms of bone and cartilage metabolism regulatory factor

genes with common skeletal disorders, such as osteoporosis and osteoarthritis. These include genes for estrogen receptor (ER), vitamin D receptor (VDR), parathyroid hormone (PTH) and interleukin-1 (IL-1) [1, 2, 4, 5, 7, 10, 12, 15, 16, 19, 20, 22, 29, 33, 35, 36]. Several investigations have suggested polymorphisms in the genes encoding ER, VDR, type II procollagen, type XI collagen and transforming growth factor-β are associated with either the development or severity of osteoarthritis of extremities [1, 4, 16, 18, 33–35]. However, there are only a few reports on the association of gene polymorphisms with spinal spondylosis [36, 37]. Indeed, several factors including late onset of the disorder, lack of a large family suitable for genetic linkage analysis, a strong contribution of environmental factors, such as accumulated mechanical stress to the spine, and a probable polygenetic nature of the disease have hampered the genetic analysis of the disorder. Hence, this study focused on the association of polymorphisms of certain candidate genes: ER, VDR, PTH and IL-1β, all of which are known to be potent regulators of skeletal metabolism, with spondylotic changes of the lumbar spine in a population of Japanese postmenopausal women.

Materials and methods

Subjects

Genotype analyses were carried out using genomic DNA extracted from peripheral blood samples obtained from 318 post-menopausal Japanese women living in Nagano prefecture. All patients were unrelated volunteers who gave informed consent before the study. Since this is a rural area located in the central Japan with little change of inhabitants, the population in each generation shares similar genetic backgrounds from the Japanese typical ethnic ancestry as previously reported [28]. The number of samples for each gene analysis was different since the content of the informed consent varied depending on the time of the sample collection; that is, at the start of this project we stated only VDR genotyping analysis in the informed consent, and added ER, IL-1β, and PTH analyses in it thereafter. The clinical characteristics of the women recruited for the study were as follows: mean ± SD of age 63.7 ± 10.0 (range 51–76) years old, body height 151.0 ± 6.5 cm, body weight: 50.8 ± 8.0 kg, and body mass index (BMI) 22.3 ± 3.1 kg/m^2. Exclusion criteria included endocrinological disorders (e.g., hyperthyroidism, hyperparathyroidism, diabetes mellitus), liver or renal diseases, use of medications that were known to affect bone and cartilage metabolism (e.g., estrogen, bisphosphonates, vitamin D, calcium supplement, corticosteroids, anticonvulsants, heparin), and unusual gynecological history. The patients were also divided into two subpopulations, younger and older groups, bordered by the average age: 63.9 years for ER, 63.6 years for VDR, 63.7 years for PTH, and 64.1 years for IL-1β.

Measurements of phenotypes

The severity of spondylosis in the disk level from L1/2 to L5/S1 was graded according to the Kellgren–Lawrence scoring (grade 0–4) on a lateral radiograph of the lumbar spine under standardized conditions. This scoring is a well-known system for grading osteoarthritis severity of many joints [17], and has widely been used in previous studies to assess the severity of lumbar spondylosis [23, 38]. The scoring is designated as follows: 0 = normal; 1 = doubtful narrowing of joint space and possible osteophyte formation; 2 = definite osteophytes and possible narrowing of joint space; 3 = moderate multiple osteophytes, definite narrowing of joint space, some sclerosis, and possible deformity of bone contour; 4 = large osteophytes, marked narrowing of joint space, severe sclerosis, and definite deformity of bone contour. Bone mineral density (BMD, mg/cm^2) of the second through fourth lumbar spine (L2–L4) was measured by dual-energy X-ray absorptiometry (DPX-L, Lunar Co., Madison, WI). This parameter was expressed as a Z score that is a deviation from the weight-adjusted average BMD of each age based on the data of 20,000 Japanese women installed in Lunar DPX-L. The study protocol was approved by the ethical committee for human subjects of the University of Tokyo.

Genomic DNA analysis for restriction fragment length polymorphism

Genomic DNA (0.1 μg) was subjected to polymerase chain reaction (PCR) amplification using Taq DNA polymerase (PE Biosystem, Foster City, CA) with the sense and antisense primers synthesized by Operon Biotechnologies Inc. (Tokyo, Japan) upon request (Table 1). PCR products were digested by restriction endonucleases: *Pvu*-II and *Xba*-I for ER, *Apa*-I and *Bsm*-I for VDR, Bst-BI and *Dra*-I for PTH, and *Aba*-I for IL-1β, and digested products were analyzed by 1.2% agarose gel electrophoresis. The allele that could be digested by the enzyme was expressed by (+) while that could not by (−), and the RFLP genotype was expressed by the combination: ++, +−, and −−. In addition to the genotypes, the haplotypes were shown as the combination of two RFLP genotypes (++ = 1, +− = 2, and −− = 3) in ER (*Pvu*-II:*Xba*-I), VDR (*Apa*-I:*Bsm*-I) or PTH (*Bst*-BI:*Dra*-I) [11, 12, 13, 21, 22, 23, 31, 32, 33]. Hardy-Weinberg equilibrium [11] was used to determine whether or not there are large departures from independence between pairs of alleles at a gene locus.

Table 1 Primers for RFLP in each candidate gene

Gene	Forward	Reverse	Product size (bp)	Annealing temperature (°C)
ER	CTGCCACCCTATCTGTATCTTTC	TCTTTCTCTGCCACCCTGGCGTCG	629	57
VDR	AGCTGGCCCTGGCACTGACTC	ATGGAAACACCTTGCTTCTTCTCCC	265	56
PTH	CATTCTGTGTACTATAGTTTG	GAGCTTTGAATTAGCAGCATG	384	54
IL-1β	CTCATATTCCTGGCTAGTTTTGCTGA	TTGAAAGCACAGTCGGGCATAC	345	56

Linkage disequilibrium among these RFLPs was evaluated by calculating haplotype frequencies according to the method by Hill [13] and Thompson et al. [32].

Statistical analyses

Means of Kellgren–Lawrence score in each genotype or haplotype were evaluated by ANOVA and significance of differences was determined by post-hoc testing using Bonferroni's method. The χ^2 test was used to assess Hardy–Weinberg equilibrium. A P value less than 0.05 was considered statistically significant.

Results

Association of ER, VDR, PTH and IL-1β RFLP genotypes with lumbar spondylosis

Table 2 shows the background data of the study participants. The genotypic frequencies for these RFLPs were not significantly different in any subpopulation from those expected for populations in Hardy–Weinberg equilibrium (all $P > 0.05$). In addition, none of the linkage disequilibrium values for marker pairs differed significantly from zero (all $P > 0.05$), indicating there was no significant linkage disequilibrium among these RFLPs.

Regarding the association of the genotypes with the background data, no significant difference in age, body weight, height or BMI was seen among the RFLP genotypes in ER, VDR, PTH or IL-1β (all $P > 0.05$). BMD (L2–4) expressed as the Z score after being adjusted by age and weight also was not different among the genotypes.

When associations between the RFLP genotypes and the severity of spondylosis determined by the Kellgren–Lawrence grading were examined, there was no significant difference of the severity among genotypes in any RFLPs at any disk level from L1/2 to L5/S1 (all $P > 0.05$, data not shown). For a stratified analysis by age, we divided the population into two groups younger and older than the average age in each genotype popu-

Table 2 Background data of women of each genotype

Gene	Enzyme	Genotype	Age (years)	Body height (cm)	Body weight (kg)	BMI	BMD (Z score)
ER ($n=261$)	*Pvu*-II	++($n=78$)	63.1 (10.1)	150.3 (6.2)	49.9 (8.5)	22.0 (3.0)	0.121 (1.433)
		+−($n=139$)	64.2 (10.7)	150.8 (7.2)	50.6 (8.0)	22.3 (3.3)	−0.006 (1.432)
		−−($n=44$)	64.5 (9.0)	151.3 (6.3)	52.4 (7.9)	22.9 (2.8)	−0.259 (1.191)
	Xba-I	++($n=176$)	63.4 (10.8)	150.5 (6.7)	50.1 (8.3)	22.1 (2.9)	0.004 (1.427)
		+−($n=79$)	64.8 (8.9)	151.5 (6.9)	52.2 (7.9)	22.8 (3.5)	−0.037 (1.360)
		−−($n=6$)	66.7 (8.2)	147.3 (4.8)	48.7 (6.3)	22.4 (2.4)	−0.047 (1.179)
VDR ($n=318$)	*Apa*-I	++($n=125$)	63.3 (9.8)	151.0 (6.9)	51.4 (8.7)	22.5 (3.5)	−0.055 (1.498)
		+−($n=149$)	64.0 (10.1)	151.1 (6.0)	50.7 (7.6)	22.2 (2.8)	0.137 (1.463)
		−−($n=44$)	63.3 (10.1)	150.3 (6.5)	49.4 (6.8)	21.9 (2.7)	−0.332 (1.206)
	Bsm-I	++($n=238$)	63.6 (9.9)	151.1 (6.5)	51.0 (8.3)	22.3 (3.2)	0.059 (1.491)
		+−($n=72$)	64.0 (10.5)	150.7 (6.2)	50.5 (7.0)	22.2 (2.6)	−0.214 (1.325)
		−−($n=8$)	62.1 (8.0)	149.1 (5.9)	46.4 (6.0)	20.9 (3.1)	−0.489 (1.110)
PTH ($n=104$)	*Bst*-BI	++($n=1$)	60 (–)	153 (–)	39 (–)	16.7 (–)	−0.700 (–)
		+−($n=14$)	62.3 (12.6)	151.8 (7.2)	51.5 (7.4)	22.3 (2.9)	−0.576 (1.262)
		−−($n=89$)	63.9 (10.4)	150.3 (6.0)	50.5 (7.2)	22.4 (3.1)	−0.142 (1.335)
	Dra-I	++($n=0$)	–	–	–	–	–
		+−($n=27$)	63.2 (12.1)	150.0 (6.1)	50.0 (7.0)	22.2 (2.6)	−0.590 (1.314)
		−−($n=77$)	63.8 (10.1)	150.7 (6.2)	50.7 (7.4)	22.3 (3.2)	−0.071 (1.307)
IL-1β ($n=116$)	*Aba*-I	++($n=44$)	64.9 (10.9)	150.7 (7.1)	50.8 (7.9)	22.4 (3.4)	−0.395 (1.248)
		+−($n=52$)	63.8 (12.5)	151.3 (5.5)	50.1 (6.3)	21.9 (2.8)	−0.059 (1.282)
		−−($n=20$)	63.1 (9.7)	149.1 (5.1)	50.0 (8.2)	22.5 (3.3)	−0.318 (1.500)

Data of age, body height, weight, BMI, BMD (L2-4, Z score) are expressed by the mean (SD)